Int. J. Cancer: **108,** 237–242 (2004)

Publication of the International Union Against Cancer

MUTATIONS OF *BRAF* ARE ASSOCIATED WITH EXTENSIVE *hMLH1* PROMOTER METHYLATION IN SPORADIC COLORECTAL CARCINOMAS

Koji KOINUMA[1,2], Kazuhisa SHITOH[1], Yasuyuki MIYAKURA[1], Taiji FURUKAWA[1], Yoshihiro YAMASHITA[2], Jun OTA[2], Ruri OHKI[2], Young Lim CHOI[2], Tomoaki WADA[2], Fumio KONISHI[3], Hideo NAGAI[1] and Hiroyuki MANO[2,4]*

[1]*Department of Surgery, Jichi Medical School, Tochigi, Japan*
[2]*Division of Functional Genomics, Jichi Medical School, Tochigi, Japan*
[3]*Department of Surgery, Omiya Medical Center, Jichi Medical School, Saitama, Japan*
[4]*Crest, Japan Science and Technology Agency, Saitama, Japan*

Activating mutations of *BRAF* have been frequently observed in microsatellite unstable (MSI$^+$) colorectal carcinomas (CRCs), in which mutations of *BRAF* and *KRAS* are mutually exclusive. Previously, we reported that hypermethylation of *hMLH1* might play an important role in the tumorigenesis of right-sided sporadic CRCs with MSI showing less frequency of *KRAS/TP53* alteration. Therefore, we have assumed that *BRAF* mutations might be highly associated with *hMLH1* methylation status rather than MSI status. In this study, mutations of *BRAF* and *KRAS* and their relationship with MSI and *hMLH1* methylation status were examined in 140 resected specimens of CRC. The methylation status was classified into 3 types: full methylation (FM), partial methylation (PM) and nonmethylation (NM). Only FM closely linked to reduced expression of hMLH1 protein. *BRAF* mutations were found in 16 cases (11%), all leading to the production of BRAF^{V599E}. As for MSI status, *BRAF* mutations were found in 43% of MSI$^+$ and 4% of MSI$^-$ cases ($p < 0.0001$). Among the MSI$^+$ individuals, *BRAF* mutations were more frequent in cases with hMLH1 deficiency (58%) than those with hMSH2 deficiency (0%; $p = 0.02$). Moreover, they were found in 69% of FM, 4% of PM and 4% of NM, revealing a striking difference between FM and the other 2 groups (FM *vs.* PM or NM; $p < 0.0001$). These findings suggest that BRAF activation may participate in the carcinogenesis of sporadic CRCs with *hMLH1* hypermethylation in the proximal colon, independently of KRAS activation.

Key words: *sporadic colorectal cancer;* BRAF *mutation;* hMLH1 *hypermethylation; microsatellite instability*

In the development of colorectal cancer (CRC), it is now widely accepted that some forms of genetic instability lead to the sequential accumulation of genetic alterations and consequently develop carcinomas.[1] RAS activation in the MAP kinase cascade is supposed to constitute a part of the primary events in colorectal carcinogenesis, and the *KRAS* gene mutations have been found in about 30–40% cases of sporadic CRCs.[2–4]

Recently, activating *BRAF* mutations have been found almost invariably in melanoma cells and sometimes in other types of carcinoma, including CRCs,[5–7] implying a function of *BRAF* as a protooncogene. The *RAF* genes are members of MAPK pathway, encoding serine/threonine kinases that integrate the upstream input signals.[8,9] Once recruited at the cell membrane by GTP-loaded RAS, RAF becomes activated and subsequently phosphorylates the downstream kinases, MEKs, which eventually induce transcriptional activation of the target genes.[9]

More recently, frequent *BRAF* mutations and infrequent *KRAS* mutations have been reported in DNA-mismatch repair (MMR)-deficient CRCs.[10] Inactivation of MMR genes incurs instability of genomic microsatellite sequence (microsatellite instability, or MSI), which is found in the majority of patients with hereditary nonpolyposis colorectal cancer syndrome (HNPCC) and in 10–15% of cases of sporadic CRCs.[11–13] Moreover, it was also reported that 70–90% of sporadic CRCs with MSI (MSI$^+$ CRCs) are associated with hypermethylation of *hMLH1*, one of DNA-MMR genes, and have distinct clinical and pathologic characteristics, *i.e.*, occurrence in older females, location in the proximal colon and histopathology of mucious or poor differentiation.[14–20]

We have previously examined the methylation status of *hMLH1* gene in sporadic CRCs by use of 5 sets of primer spanning the whole CpG sites within its promoter region and have classified the methylation status into 3 subtypes: full methylation, partial methylation and nonmethylation.[21,22] We reported that an extensive methylation, or full methylation, of *hMLH1* promoter was found in about 80% of MSI$^+$ CRC cases and was highly associated with loss of expression of its gene product. Interestingly, this type of CRC cells are rarely associated with *KRAS* mutations and loss of heterozygosity (LOH) of *TP53* gene.[22] It is therefore possible that extensive methylation of *hMLH1* promoter region may contribute to the carcinogenesis of the right-sided sporadic CRCs, independently of *KRAS/p53* alterations.

From these results, 2 questions may arise. First, does the activation of BRAF, instead of KRAS, take part in the carcinogenesis of CRCs with extensive *hMLH1* methylation? Second, if so, does the BRAF activation have any relationship with the CRCs with partial methylation, although most of which are microsatellite stable (MSI$^-$), maintain MMR gene expression and show a relatively high incidence of KRAS and p53 alterations?[22]

Additionally, in the melanoma cells, high frequency of mutations of *β-catenin* and *BRAF* has been recognized.[23] Some researchers previously reported that *β-catenin* mutations were more common in MSI$^+$ CRCs than in MSI$^-$ ones.[19,23–25] However, it has not been elucidated yet whether there are any relationship between the mutations of *β-catenin* and *BRAF* in the CRCs with *hMLH1* hypermethylation.

In this study, we have investigated the frequency of *BRAF* mutation and its relationship with *KRAS* and *β-catenin* mutations in a large consecutive series of sporadic CRCs in regard to both MSI status and degrees of *hMLH1* methylation.

Abbreviations: CRC, colorectal cancer; FM, full methylation; HNPCC, hereditary nonpolyposis colorectal cancer syndrome; LOH, loss of heterozygosity; MAPK, mitogen-activated protein kinase; MAPKKK, mitogen-activated protein kinase kinase kinases; MEK, mitogen-activated protein/extracellular signal-regulated kinase kinase; MGMT, O^6-methylguanine DNA methyltransferase; MMR, mismatch repair; MSI, microsatellite instability; NM, nonmethylation; PM, partial methylation.

*Correspondence to: Division of Functional Genomics, Jichi Medical School, 3311-1 Yakushiji, Minamikawachi-machi, Kawachi-gun, Tochigi 329-0498, Japan. Fax: +81-285-44-7322. E-mail: hmano@jichi.ac.jp

Received 23 May 2003; Revised 4 August 2003; Accepted 25 August 2003

DOI 10.1002/ijc.11523
Published online 27 October 2003 in Wiley InterScience (www.interscience.wiley.com).

MATERIAL AND METHODS

Tumor samples

Tumor samples were obtained from 140 sporadic CRC patients who underwent surgical treatment at the Jichi Medical School Hospital. None of the patients had first-degree relatives with CRC. Informed consents were obtained from all patients, and the ethics committee of the Jichi Medical School approved this study (#02-01). We selected these cases from approximately 380 consecutive series of CRCs previously analyzed for MSI status.[21,26] All the MSI^+ cases were reconfirmed for the MSI status by pentaplex PCR method, whereas MSI^- CRCs were selected so that the gender and tumor site were balanced between the MSI^+ and MSI^- groups (MSI^+, $n = 28$; MSI^-, $n = 112$). The patients were 69 men and 71 women, and their age ranged from 19 to 86 years with a mean of 63 years.

DNA extraction

Genomic DNA was extracted from fresh-frozen samples of tumor by use of QIAamp DNA Mini Kit (Qiagen, Chatsworth, CA) according to the manufacturer's protocol.

BRAF *mutation analysis*

BRAF mutations were analyzed in exons 11 and 15. These exons were chosen because all reported *BRAF* mutations occurred at these regions. PCR was performed with 2–5 ng of genomic DNA as a template by using the same PCR primer as reported previously.[5] PCR condition was as follows: 94°C for 9 min, followed by 35 cycles of 94°C for 1 min, 60°C for 1 min and 72°C for 2 min. The PCR products were purified using a QIAquick spin purification kit (Qiagen), and the purified PCR products were sequenced with BigDye Terminator Cycle Sequencing Ready Reaction kits (PE Applied Biosystems, Foster City, CA), all according to the manufacturers' instructions. Sequencing was performed in both directions using forward and reverse PCR primers. The purified products were run on an ABI 310 PRISM Genetic Analyzer (PE Applied Biosystems). The data were collected and analyzed using the Applied Biosystems sequencing analysis software.

MSI status analysis

MSI was analyzed by using 9 microsatellite repeat loci (3 markers were dinucleotide repeats and 6 were mononucleotide repeats) as described previously.[21] MSI status was stratified as follows according to the criteria of the National Cancer Institute (NCI) workshop.[27] High-frequency MSI (MSI-H) was defined as the alterations of microsatellite repeat were found in more than 40% of examined markers or in 2 or more NCI-recommended markers. Low-frequency MSI (MSI-L) was defined as the alterations in less than 40% or only one NCI-recommended marker. If no alterations of any examined markers were found, tumors were defined as microsatellite stable (MSS). In this study, we defined MSI-H as MSI-positive (MSI^+), and both MSI-L and MSS as MSI-negative (MSI^-), because only the MSI-H phenotype in sporadic CRCs is associated with true MMR defects and distinctive clinicopathologic features.[28,29] For the precision of MSI status, we reexamined all MSI^+ samples by pentaplex PCR method using 5 quasimonomorphic mononucleotide repeats, because this method has been reported to be simpler to use and show higher sensitivity and specificity.[30]

Analysis of methylation status of hMLH1 *promoter region*

Analysis of methylation status of *hMLH1* gene was performed by Na-bisulfite treatment and PCR single-strand conformation polymorphism (SSCP) analysis (BiPS) as described previously.[21] In brief, 5 sets of primers comprising the whole CpG sites within the *hMLH1* promoter region were prepared (Fig. 1), and methylated and unmethylated DNA amplicons were separated through SSCP analysis. When the bands showed mobility shifts, they were cut from the gels and subsequently sequenced directly by use of an ABI 310 PRISM Genetic Analyzer. Primer sequences and PCR conditions were utilized as reported previously.[21] The methylation patterns were defined as full methylation if all the CpG sites within the promoter regions showed methylation; as partial methylation if some CpG sites in the upstream region showed methylation; and as nonmethylation if no CpG sites in the region showed methylation.

KRAS *mutation analysis*

KRAS mutations were analyzed by direct sequencing at codons 12 and 13 of *KRAS* by using its genomic DNA. First, a flanking PCR product of 179 bp was amplified (annealing temperature was 58°C) using the primers 5′-AGGCCTGCTGAAAATGACTGAATA-3′ (sense) and 5′-CTGTATCAAAGAATGGTCCTGCAC-3′ (antisense). The resulting fragment was then used as a template to amplify a 114 bp fragment, including codons 12 and 13 using the primers 5′-AAAATGACTGAATATAAACTTGTGG-3′ (sense) and 5′-CTCTATTGTTGGATCATATTCGTC-3′ (antisense; annealing temperature was 50°C). The PCR product was sequenced by the same method as in the *BRAF* mutation analysis.

β-catenin *mutation analysis*

Mutations in *β-catenin* were analyzed by direct sequencing at its exon 3, in which the majority of mutation hot spots were included. The PCR primers were 5′-GATTTGATGGAGTTGGACATGG-3′ (sense) and 5′-TGTTCTTGAGTGAAGGACTGAG-3′ (antisense; annealing temperature was 63°C). The direct sequencing of the PCR product was performed by the same method as in the *BRAF* mutation analysis.

Immunohistochemical analysis

Immunohistochemical analysis for both hMLH1 and hMSH2 expression was performed on all MSI^+ tumor samples as described previously.[26]

Statistical analysis

Statistical analyses for variable results were performed by Fisher's exact test and Student's *t*-test. Probability values below 0.05 were considered to be statistically significant (StatView J 5.0 software, Abacus Concepts, Berkeley, CA).

RESULTS

Clinicopathologic features of patients with BRAF *mutations*

We identified 16 patients whose CRCs showed *BRAF* mutations (Table I). All the mutations resulted in a V599E substitution in the

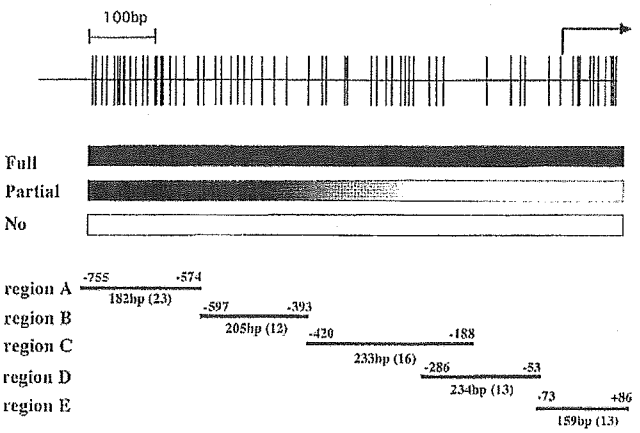

FIGURE 1 – Top: Schematic presentation of the *MLH1* promoter region. Middle: Full methylation (all CpG sites in regions A–E show methylation), partial methylation (some CpG sites in upstream region show methylation) and nonmethylation (no CpG site shows methylation). Bottom: Design of the PCR primers and the PCR products for regions A–E. Their positions relative to the adenine residue at the start codon and the size of the amplified DNA fragments are shown. Numbers in parenthesis indicate the number of CpG sites within each region.

BRAF protein (Fig. 2). None of the cases had *BRAF* mutations in the normal colonic mucosa positioned far away from the cancer area, implying that the *BRAF* mutations should be a somatic event. The mean age of cancer onset in the patients with *BRAF* mutations was older than those without *BRAF* mutations, although the difference was not statistically significant: 73.1 ± 10.5 years compared with 62.5 ± 12.5 years ($p = 0.06$, Student's *t*-test; Table II). Gender distribution was also different between these 2 groups, with females comprising 75% (12/16) of the *BRAF* mutation group and 48% (59/124) of the nonmutation group ($p = 0.06$, Fisher's exact test; Table II). The tumor with *BRAF* mutation cases was more frequently located in the proximal colon (94%; 15/16) than that with nonmutation ones (37%; 46/124; $p < 0.0001$, Fisher's exact test; Table II).

BRAF *mutations and MSI status*

BRAF mutations were found in 43% (12/28) of MSI^+ CRCs and 4% (4/112) of MSI^- CRCs ($p < 0.0001$, Fisher's exact test; Table III).

BRAF *mutations and MMR protein expression*

BRAF mutations were more common in the tumors showing reduced hMLH1 protein expression (58%; 11/19) than those showing reduced hMSH2 expression (0%; 0/6; $p = 0.02$, Fisher's exact test; Table IV).

BRAF *mutations and* hMLH1 *promoter methylation status*

BRAF mutations were found in 69% (11/16) of full methylation, 4% (2/45) of partial methylation and 4% (3/79) of nonmethylation (Table V). The ratio of *BRAF* mutations was statistically significant between full and partial as well as between full and none ($p < 0.0001$, Fisher's exact test).

KRAS *mutations*

KRAS mutations were identified in 38 cases. Two cases with *KRAS* mutations were in MSI^+ (7%; 2/28) and 36 cases were in MSI^- (32%; 36/112; $p = 0.008$, Fisher's exact test; Table III). Regarding the methylation status, *KRAS* mutations were not found

TABLE I – ALL CRC CASES WITH *BRAF* MUTATIONS

Patient no.	Age (yr)	Gender	Site	MSI	*hMLH1* methylation	*BRAF* amino acid	*KRAS*	β-*catenin*	Dukes' stage	Histologic grade
225	83	F	P	+	Full	V599E	Wild	Wild	C	Well
263	86	F	P	+	Full	V599E	Wild	Wild	B	Moderate
268	85	F	P	+	Full	V599E	Wild	Wild	B	Poor
280	83	F	P	+	Full	V599E	Wild	Wild	C	Well
305	74	M	P	+	Full	V599E	Wild	Wild	B	Poor
318	76	F	P	+	Full	V599E	Wild	Wild	B	Well
336	68	M	P	+	Full	V599E	Wild	Wild	B	Mucinous
413	69	F	P	+	Full	V599E	Wild	Wild	B	Well
416	76	F	P	+	Full	V599E	Wild	Wild	B	Mucinous
479	74	F	P	+	Full	V599E	Wild	Wild	B	Moderate
507	64	M	P	+	Full	V599E	Wild	Wild	A	Moderate
274	81	M	D	−	Partial	V599E	Wild	Wild	B	Moderate
328	52	F	P	−	Partial	V599E	Wild	Wild	B	Moderate
293	70	F	P	−	Non	V599E	Wild	Wild	D	Mucinous
384	77	F	P	+	Non	V599E	Wild	Wild	A	Poor
509	51	F	P	−	Non	V599E	Wild	Wild	C	Poor

P, proximal colon; D, distal colon; Full, full methylation; Partial, partial methylation; Non, nonmethylation; Well, well-differentiated adenocarcinoma; Mod, moderately differentiated adenocarcinoma; Poor, poorly differentiated adenocarcinoma; Muc, mucinous carcinoma.

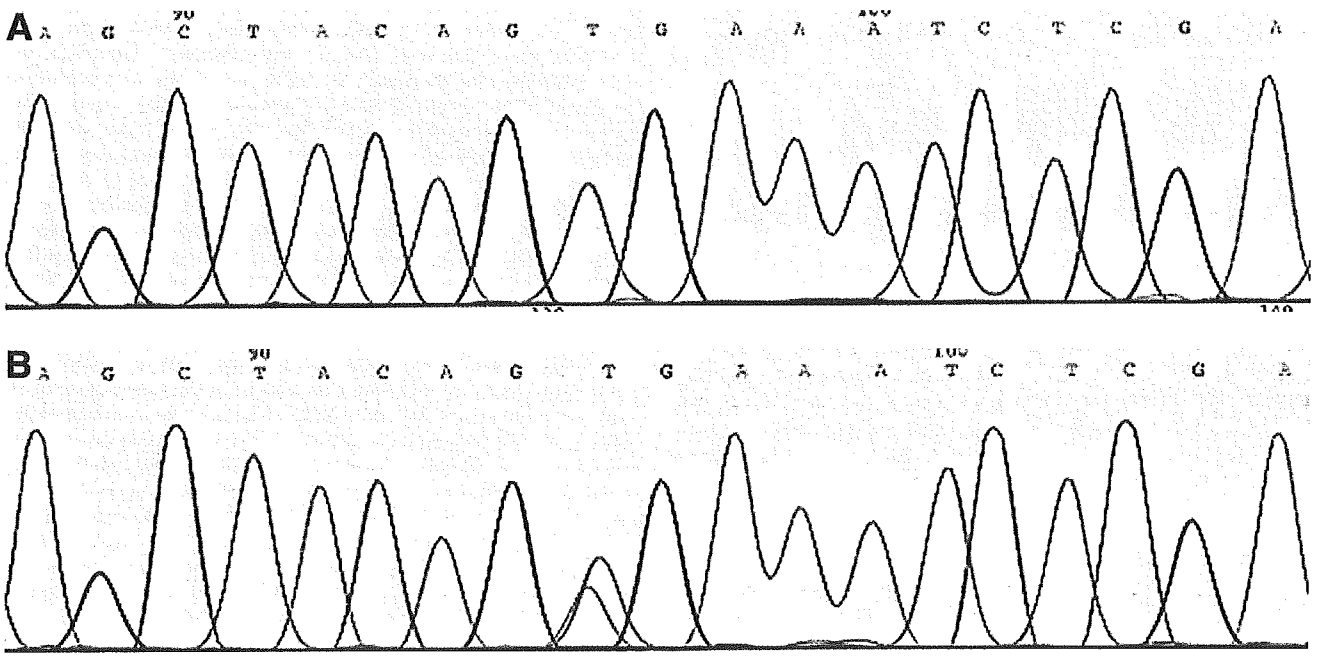

FIGURE 2 – (*a*) Representative sequence chromatographs from *BRAF* exon 15 showing wild type. (*b*) T1796A transversion resulting in a V599E substitution.

TABLE II – CLINICOPATHOLOGIC FEATURES OF *BRAF* MUTATION CASES

	BRAF mutation (n = 16) (%)	Non-*BRAF* mutation (n = 124) (%)	P-value
Age (yr)	73.1 ± 10.5	62.5 ± 12.5	0.06
Gender			0.06
Male	4 (25)	65 (52)	
Female	12 (75)	59 (48)	
Tumor site			< 0.0001
Proximal	15 (94)	46 (37)	
Distal	1 (6)	78 (63)	
Dukes' stage			0.07
A/B	12 (75)	59 (50)	
C/D	4 (25)	59 (50)	
Histologic grade			0.0008
Well/moderate	9 (56)	109 (92)	
Poor/mucinous	7 (44)	10 (8)	

Well, well-differentiated adenocarcinoma; moderate, moderately differentiated adenocarcinoma; Poor, poorly differentiated adenocarcinoma; mucinous, mucinous carcinoma.

TABLE III – MSI STATUS AND MUTATIONS OF *BRAF*, *KRAS* AND β-*CATENIN*

MSI status	*BRAF* mutation (%)	*KRAS* mutation (%)	β-*catenin* mutation (%)
MSI^+	42.9 (12/28)[a]	7.1 (2/28)[b]	7.1 (2/28)
MSI^-	3.6 (4/112)[a]	32.1 (36/112)[b]	2.7 (3/112)
Total	11.4 (16/140)	27.1 (38/140)	3.6 (5/140)

[a]Fisher's exact test, $p < 0.0001$.–[b]Fisher's exact test, $p = 0.008$.

TABLE IV – *BRAF* MUTATION AND MMR PROTEIN EXPRESSION

	Number of cases	*BRAF* mutation (%)
hMLH1-deficient	19	57.9 (11/19)[a]
hMSH2-deficient	6	0 (0/6)[a]

[a]Fisher's exact test, $p = 0.02$.

TABLE V – *hMLH1* METHYLATION STATUS AND MUTATIONS OF *BRAF*, *KRAS* AND β-*CATENIN*

hMLH1 methylation status	*BRAF* mutation (%)	*KRAS* mutation (%)	β-*catenin* mutation (%)
Full methylation	68.8 (11/16)[a,b]	0 (0/16)[c,d]	0 (0/16)
Partial methylation	4.4 (2/45)[a]	37.8 (17/45)[c]	0 (0/45)
Nonmethylation	3.8 (3/79)[b]	26.6 (21/79)[d]	6.3 (5/79)
Total	11.4 (16/140)	27.1 (38/140)	3.6 (5/140)

[a]Fisher's exact test, $P < 0.0001$.–[b]Fisher's exact test, $P < 0.0001$.–[c]Fisher's exact test, $P = 0.003$.–[d]Fisher's exact test, $P = 0.02$.

(0%; 0/16) in any of the full methylation cases, but were found in 17 of the partial methylation patients (38%; 17/45) and 21 of the nonmethylation group (26.6%; 21/79), which was consistent with our previous results[21] (Table V). The ratio of *KRAS* mutations was significantly different between full and partial and between full and none cases ($p = 0.003$ and 0.02, respectively, Fisher's exact test). None of the cases with *BRAF* mutations exhibited *KRAS* mutations simultaneously.

β-catenin *mutations*

β-catenin mutations were found in 5 cases. Two cases were in MSI^+ (7%; 2/28) and 3 cases were in MSI^- (3%; 3/112; $p = 0.26$, Fisher's exact test; Table III). However, none of the cases with full or partial methylation showed *β-catenin* mutations, and there were no cases exhibiting both *BRAF* and *β-catenin* mutations simultaneously (Table V).

DISCUSSIONS

The MAPK pathway plays a crucial role in the signal transduction of many hormones, growth factors and differentiation factors.[31,32] At the level of MAPKKKs, several RAF family members exist, that is, ARAF, BRAF and RAF1 with divergent tissue specificity and upstream regulation.[33] The 3 proteins are thought to have uneven ability to activate MEK, and BRAF has been identified as the major MEK activator.[32]

Recently, *BRAF* activating mutations were observed in some proportion of human carcinomas, especially in melanoma, lung cancer, as well as colon cancer.[5–7] *BRAF* gene was therefore supposed to be a novel protooncogene that might contribute to the tumorigenesis in these types of transformed cells. Interestingly, the mutational spots of *BRAF* gene cluster within the activation segment (exon 15) and the G-loop (exon 11) of the kinase domain, which are highly conserved among serine/threonine kinases throughout evolution.[5] Activating mutations in these hot spots are supposed to increase its kinase activity and subsequently urge to phosphorylate the downstream kinase, MEK. V599 is the major site of point mutations in the BRAF protein and V599E acidic substitution has been commonly found in melanoma, colon cancer and ovarian cancer cells.[5] Intriguingly, the tumors with $BRAF^{V599E}$ showed no *KRAS* mutations simultaneously, although non-V599E cases were sometimes coincident with *KRAS* mutations.[5,10,34] It has been hypothesized therefore that V599E might mimic the phosphorylation of T598 of BRAF that constitutes the natural activation mechanism of this protein. Because of its potent kinase activity, BRAF with this type of mutation might have no need to depend on RAS for the initiation of the MAP kinase pathway activation.

In our series of sporadic CRCs, 28 cases showed MSI^+, in which 19 were with hMLH1 deficiency and 6 were with hMSH2 deficiency. *BRAF* mutations were more frequent in MSI^+ CRCs than in MSI^- CRCs (43%, 12/28 *vs.* 4%, 4/112; $p < 0.0001$). This result was nearly consistent with that in the previous report.[10] Interestingly, *BRAF* mutations were more frequent in hMLH1-deficient cases than hMSH2-deficient ones (58%, 11/19 *vs.* 0%, 0/6; $p = 0.02$). It has been widely accepted that MSI in sporadic CRCs commonly results from epigenetic silencing of *hMLH1* gene, secondary to its promoter methylation, and 70–90% of MSI^+ CRCs indeed show hypermethylation of the *hMLH1* gene.[15,21,35] Moreover, extensive methylation of *hMLH1* promoter is closely correlated with hMLH1 inactivation.[21] Therefore, we have examined the frequency of *BRAF* mutations with regard to the methylation status of *hMLH1* promoter region. Amazingly, *BRAF* mutations were extremely frequent in the cases with full methylation compared to those without full methylation (69%, 11/16 *vs.* 4%, 5/124; $p < 0.0001$). As generally seen in the cases with *hMLH1* methylation, the CRCs with *BRAF* mutations were more frequent in older females, commonly located in the proximal colon, and showed the histopathology of mucinous or poor differentiation. Our data suggest that the activating mutation of *BRAF* may be highly associated with an extensive methylation of *hMLH1* gene.

In a recent study, we proposed that the shift of methylation status from partial to full might be critical in the tumorigenesis of right-sided sporadic CRCs with MSI, because more than half of the cases with full methylation showed partial methylation in their normal mucosa far from the tumor.[21] However, the cancers with partial methylation not yet reaching full methylation showed distinct clinical and biologic features from those with full methylation, with relatively high frequency in the alterations of *KRAS/p53*.[22] In this study, *BRAF* mutations were less frequent in the cases with partial methylation compared to those with full methylation (4%, 2/45 *vs.* 69%, 11/16; $p < 0.0001$). We state that partial methylation is not generally the true pathogenic methylation status of *hMLH1* gene.

In our study, all the mutations of *BRAF* resulted in V599E substitutions (T-to-A transversion at nucleotide 1796). Rajago-

palan *et al.*[10] reported that all but one of the 15 *BRAF* mutations in MMR-deficient cases resulted in V599E. O^6-methylguanine DNA methyltransferase (MGMT) is a DNA repair protein and MGMT epigenetic inactivation by its promoter hypermethylation is supposed to cause G-to-A transition mutation in *KRAS* and G:C-to-A:T transition mutation in *p53*. Indeed, 71% cases with *KRAS* and *p53* mutations showed hypermethylation of *MGMT*.[36,37] Therefore, it might be possible that inactivation of an anonymous DNA-repair gene by promoter hypermethylation has an association with A-to-T transition mutation in *BRAF* gene.

Yuen *et al.*[34] have reported that there are many similarities between the phenotypic patterns of CRCs with *KRAS* and *BRAF* mutations. However, they showed that the cases with *BRAF* mutations differ from those with *KRAS* mutations in the Dukes' stage. Consistent with their results, the cases with *BRAF* mutations in our study were more common with Dukes' A/B grades than with Dukes' C/D, although the difference was not statistically significant ($p = 0.07$, Fisher's exact test). Moreover, the patients with *BRAF* mutations were approximately 13 years older than those with *KRAS* mutations (data not shown). Therefore, we speculate that the CRCs with *BRAF* mutations may belong to a clinical entity distinct from one of CRCs with *KRAS* mutations.

In melanoma cells as well as MSI^+ CRC cells, high frequency of *β-catenin* and *BRAF* mutations have been reported.[19,23–25] In this study, *β-catenin* mutations were uncommon in both MSI^+ (7%; 2/28) and MSI^- (3%; 3/112), as reported previously by Jass *et al.*[29] Moreover, none of our cases with full or partial methylation showed *β-catenin* mutations. There were no cases harboring *BRAF* and *β-catenin* mutations simultaneously, implying that *β-catenin* mutation may have no association with *hMLH1* hypermethylation with regard to CRC carcinogenesis.

We previously proposed that extensive methylation of *hMLH1* promoter might play a crucial role in tumorigenesis in the proximal colon.[21] In this study, we additionally demonstrated that the activating mutations of *BRAF* might take part in the carcinogenesis of sporadic CRCs with *hMLH1* hypermethylation in the proximal colon, independently of KRAS activation. However, one question remains to be addressed. At which stage does BRAF activation contribute to malignant transformation of colon epithelial cells? Hyperplastic polyps and serrated adenomas in the right-sided colon show high frequency of *hMLH1* hypermethylation, and these lesions have been presumed to be premalignant lesions of right-sided CRCs with MSI.[29] It would be interesting to examine whether the majority of such hyperplastic polyps and serrated adenomas already have *BRAF* mutations. If most of the CRCs with extensive methylation are associated with $BRAF^{V599E}$, such subtype would be a good target for novel anticancer drugs acting on the MAPK pathway.[38,39]

ACKNOWLEDGEMENTS

The authors thank the staff of the Division of Functional Genomics, Jichi Medical School, for their helpful advice.

REFERENCES

1. Kinzler KW, Vogelstein B. Lessons from hereditary colorectal cancer. Cell 1996;87:159–70.
2. Aaltonen LA, Peltomaki P, Leach FS, Sistonen P, Pylkkanen L, Mecklin JP, Jarvinen H, Powell SM, Jen J, Hamilton SR, Petersen GM, Kinzler KW, et al. Clues to the pathogenesis of familial colorectal cancer. Science 1993;260:812–6.
3. Bos JL, Fearon ER, Hamilton SR, Verlaan-de Vries M, van Boom JH, van der Eb AJ, Vogelstein B. Prevalence of ras gene mutations in human colorectal cancers. Nature 1987;327:293–7.
4. Forrester K, Almoguera C, Han K, Grizzle WE, Perucho M. Detection of high incidence of K-ras oncogenes during human colon tumorigenesis. Nature 1987;327:298–303.
5. Davies H, Bignell GR, Cox C, Stephens P, Edkins S, Clegg S, Teague J, Woffendin H, Garnett MJ, Bottomley W, Davis N, Dicks E, et al. Mutations of the BRAF gene in human cancer. Nature 2002;417:949–54.
6. Pollock PM, Meltzer PS. A genome-based strategy uncovers frequent BRAF mutations in melanoma. Cancer Cell 2002;2:5–7.
7. Brose MS, Volpe P, Feldman M, Kumar M, Rishi I, Gerrero R, Einhorn E, Herlyn M, Minna J, Nicholson A, Roth JA, Albelda SM, et al. BRAF and RAS mutations in human lung cancer and melanoma. Cancer Res 2002;62:6997–7000.
8. Vojtek AB, Der CJ. Increasing complexity of the Ras signaling pathway. J Biol Chem 1998;273:19925–8.
9. Magee T, Marshall C. New insights into the interaction of Ras with the plasma membrane. Cell 1999;98:9–12.
10. Rajagopalan H, Bardelli A, Lengauer C, Kinzler KW, Vogelstein B, Velculescu VE. Tumorigenesis: RAF/RAS oncogenes and mismatch-repair status. Nature 2002;418:934.
11. Aaltonen LA, Peltomaki P, Mecklin JP, Jarvinen H, Jass JR, Green JS, Lynch HT, Watson P, Tallqvist G, Juhola M. Replication errors in benign and malignant tumors from hereditary nonpolyposis colorectal cancer patients. Cancer Res 1994;54:1645–8.
12. Fishel R, Lescoe MK, Rao MR, Copeland NG, Jenkins NA, Garber J, Kane M, Kolodner R. The human mutator gene homolog MSH2 and its association with hereditary nonpolyposis colon cancer. Cell 1993;75:1027–38.
13. Bronner CE, Baker SM, Morrison PT, Warren G, Smith LG, Lescoe MK, Kane M, Earabino C, Lipford J, Lindblom A, Tannergard P, Bollag RJ, et al. Mutation in the DNA mismatch repair gene homologue hMLH1 is associated with hereditary non-polyposis colon cancer. Nature 1994;368:258–61.
14. Kane MF, Loda M, Gaida GM, Lipman J, Mishra R, Goldman H, Jessup JM, Kolodner R. Methylation of the hMLH1 promoter correlates with lack of expression of hMLH1 in sporadic colon tumors and mismatch repair-defective human tumor cell lines. Cancer Res 1997;57:808–11.
15. Cunningham JM, Christensen ER, Tester DJ, Kim CY, Roche PC, Burgart LJ, Thibodeau SN. Hypermethylation of the hMLH1 promoter in colon cancer with microsatellite instability. Cancer Res 1998;58:3455–60.
16. Veigl ML, Kasturi L, Olechnowicz J, Ma AH, Lutterbaugh JD, Periyasamy S, Li GM, Drummond J, Modrich PL, Sedwick WD, Markowitz SD. Biallelic inactivation of hMLH1 by epigenetic gene silencing, a novel mechanism causing human MSI cancers. Proc Natl Acad Sci USA 1998;95:8698–702.
17. Kuismanen SA, Holmberg MT, Salovaara R, Schweizer P, Aaltonen LA, de La Chapelle A, Nystrom-Lahti M, Peltomaki P. Epigenetic phenotypes distinguish microsatellite-stable and -unstable colorectal cancers. Proc Natl Acad Sci USA 1999;96:12661–6.
18. Malkhosyan SR, Yamamoto H, Piao Z, Perucho M. Late onset and high incidence of colon cancer of the mutator phenotype with hypermethylated hMLH1 gene in women. Gastroenterology 2000;119:598.
19. Young J, Simms LA, Biden KG, Wynter C, Whitehall V, Karamatic R, George J, Goldblatt J, Walpole I, Robin SA, Borten MM, Stitz R, et al. Features of colorectal cancers with high-level microsatellite instability occurring in familial and sporadic settings: parallel pathways of tumorigenesis. Am J Pathol 2001;159:2107–16.
20. Hawkins N, Norrie M, Cheong K, Mokany E, Ku SL, Meagher A, O'Connor T, Ward R. CpG island methylation in sporadic colorectal cancers and its relationship to microsatellite instability. Gastroenterology 2002;122:1376–87.
21. Miyakura Y, Sugano K, Konishi F, Ichikawa A, Maekawa M, Shitoh K, Igarashi S, Kotake K, Koyama Y, Nagai H. Extensive methylation of hMLH1 promoter region predominates in proximal colon cancer with microsatellite instability. Gastroenterology 2001;121:1300–9.
22. Miyakura Y, Sugano K, Konishi F, Fukayama N, Igarashi S, Kotake K, Matsui T, Koyama Y, Maekawa M, Nagai H. Methylation profile of the MLH1 promoter region and their relationship to colorectal carcinogenesis. Genes Chromosomes Cancer 2003;36:17–25.
23. Sparks AB, Morin PJ, Vogelstein B, Kinzler KW. Mutational analysis of the APC/beta-catenin/Tcf pathway in colorectal cancer. Cancer Res 1998;58:1130–4.
24. Shitoh K, Furukawa T, Kojima M, Konishi F, Miyaki M, Tsukamoto T, Nagai H. Frequent activation of the beta-catenin-Tcf signaling pathway in nonfamilial colorectal carcinomas with microsatellite instability. Genes Chromosomes Cancer 2001;30:32–7.
25. Mirabelli-Primdahl L, Gryfe R, Kim H, Millar A, Luceri C, Dale D, Holowaty E, Bapat B, Gallinger S, Redston M. Beta-catenin mutations are specific for colorectal carcinomas with microsatellite instability but occur in endometrial carcinomas irrespective of mutator pathway. Cancer Res 1999;59:3346–51.
26. Furukawa T, Konishi F, Masubuchi S, Shitoh K, Nagai H, Tsukamoto T. Densely methylated MLH1 promoter correlates with decreased mRNA expression in sporadic colorectal cancers. Genes Chromosomes Cancer 2002;35:1–10.

27. Boland CR, Thibodeau SN, Hamilton SR, Sidransky D, Eshleman JR, Burt RW, Meltzer SJ, Rodriguez-Bigas MA, Fodde R, Ranzani GN, Srivastava S. A National Cancer Institute workshop on microsatellite instability for cancer detection and familial predisposition: development of international criteria for the determination of microsatellite instability in colorectal cancer. Cancer Res 1998;58:5248–57.
28. Konishi M, Kikuchi-Yanoshita R, Tanaka K, Muraoka M, Onda A, Okumura Y, Kishi N, Iwama T, Mori T, Koike M, Ushio K, Chiba M, et al. Molecular nature of colon tumors in hereditary nonpolyposis colon cancer, familial polyposis, and sporadic colon cancer. Gastroenterology 1996;111:307–17.
29. Jass JR, Biden KG, Cummings MC, Simms LA, Walsh M, Schoch E, Meltzer SJ, Wright C, Searle J, Young J, Leggett BA. Characterisation of a subtype of colorectal cancer combining features of the suppressor and mild mutator pathways. J Clin Pathol 1999;52:455–60.
30. Suraweera N, Duval A, Reperant M, Vaury C, Furlan D, Leroy K, Seruca R, Iacopetta B, Hamelin R. Evaluation of tumor microsatellite instability using five quasimonomorphic mononucleotide repeats and pentaplex PCR. Gastroenterology 2002;123:1804–11.
31. Kolch W. Meaningful relationships: the regulation of the Ras/Raf/MEK/ERK pathway by protein interactions. Biochem J 2000;351(Pt 2):289–305.
32. Peyssonnaux C, Eychene A. The Raf/MEK/ERK pathway: new concepts of activation. Biol Cell 2001;93:53–62.
33. Barnier JV, Papin C, Eychene A, Lecoq O, Calothy G. The mouse B-raf gene encodes multiple protein isoforms with tissue-specific expression. J Biol Chem 1995;270:23381–9.
34. Yuen ST, Davies H, Chan TL, Ho JW, Bignell GR, Cox C, Stephens P, Edkins S, Tsui WW, Chan AS, Futreal PA, Stratton MR, et al. Similarity of the phenotypic patterns associated with BRAF and KRAS mutations in colorectal neoplasia. Cancer Res 2002;62:6451–5.
35. Herman JG, Umar A, Polyak K, Graff JR, Ahuja N, Issa JP, Markowitz S, Willson JK, Hamilton SR, Kinzler KW, Kane MF, Kolodner RD, et al. Incidence and functional consequences of hMLH1 promoter hypermethylation in colorectal carcinoma. Proc Natl Acad Sci USA 1998;95:6870–5.
36. Esteller M, Toyota M, Sanchez-Cespedes M, Capella G, Peinado MA, Watkins DN, Issa JP, Sidransky D, Baylin SB, Herman JG. Inactivation of the DNA repair gene O6-methylguanine-DNA methyltransferase by promoter hypermethylation is associated with G to A mutations in K-ras in colorectal tumorigenesis. Cancer Res 2000;60:2368–71.
37. Esteller M, Risques RA, Toyota M, Capella G, Moreno V, Peinado MA, Baylin SB, Herman JG. Promoter hypermethylation of the DNA repair gene O(6)-methylguanine-DNA methyltransferase is associated with the presence of G:C to A:T transition mutations in p53 in human colorectal tumorigenesis. Cancer Res 2001;61:4689–92.
38. Lee JT Jr, McCubrey JA. The Raf/MEK/ERK signal transduction cascade as a target for chemotherapeutic intervention in leukemia. Leukemia 2002;16:486–507.
39. Sebolt-Leopold JS. Development of anticancer drugs targeting the MAP kinase pathway. Oncogene 2000;19:6594–9.

ACADEMIC PRESS

Available online at www.sciencedirect.com

SCIENCE DIRECT®

Biochemical and Biophysical Research Communications 307 (2003) 771–777

BBRC

www.elsevier.com/locate/ybbrc

DNA microarray analysis of in vivo progression mechanism of heart failure☆

Shuichi Ueno,[a,b] Ruri Ohki,[a,b] Toru Hashimoto,[a,b] Toshihiro Takizawa,[c] Koichi Takeuchi,[c] Yoshihiro Yamashita,[a] Jun Ota,[a,d] Young Lim Choi,[a] Tomoaki Wada,[a] Koji Koinuma,[a] Keiji Yamamoto,[b] Uichi Ikeda,[b] Kazuyuki Shimada,[b] and Hiroyuki Mano[a,d,*]

[a] *Division of Functional Genomics, Jichi Medical School, 3311-1 Yakushiji, Kawachi-gun, Tochigi 329-0498, Japan*
[b] *Division of Cardiology, Jichi Medical School, 3311-1 Yakushiji, Kawachi-gun, Tochigi 329-0498, Japan*
[c] *Department of Anatomy, Jichi Medical School, 3311-1 Yakushiji, Kawachi-gun, Tochigi 329-0498, Japan*
[d] *CREST, JST, Saitama 332-0012, Japan*

Received 11 June 2003

Abstract

Dahl salt-sensitive rats are genetically hypersensitive to sodium intake. When fed a high sodium diet, they develop systemic hypertension, followed by cardiac hypertrophy and finally heart failure within a few months. Therefore, Dahl rats represent a good model with which to study how heart failure is developed in vivo. By using DNA microarray, we here monitored the transcriptome of >8000 genes in the left ventricular muscles of Dahl rats during the course of cardiovascular damage. Expression of the atrial natriuretic peptide gene was, for instance, induced in myocytes by sodium overload and further enhanced even at the heart failure stage. Interestingly, expression of the gene for the D-binding protein, an apoptotic-related transcriptional factor, became decreased upon the transition to heart failure. To our best knowledge, this is the first report to describe the transcriptome of cardiac myocytes during the disease progression of heart failure.

Keywords: DNA microarray; Dahl salt-sensitive rat; DBP; Heart failure; Hypertension

A variety of conditions including pressure or volume overload lead to hypertrophy of cardiac muscles, which is often accompanied with an increase in systemic blood pressure (BP). The hypertrophic change is in some cases the result of a compensatory mechanism and in other cases due to yet unidentified causes. Regardless of the etiology, however, sustained hypertrophy of cardiac myocytes eventually induces a reduction in contractile ability and/or a decrease in the number of viable myocytes; the condition referred to as "heart failure" [1]. Even today, it is difficult to control the function of failed heart and this condition remains one of the leading causes of human death [2]. The possibility of preventing the progression from cardiac hypertrophy to heart failure would be greatly increased by characterization of this process at the molecular level.

Unfortunately, however, little information has been provided on this issue. Studies with neonatal rat cardiac myocytes cultured in vitro, for example, have provided important insight into the mechanism by which these cells become hypertrophic in response to various conditions [3]. However, the clarification of the next step, transition to pumping failure, should require the analysis of in vivo specimens from both hypertrophic and failed hearts. Sampling of ventricle myocytes from human patients is very difficult, especially in a large scale or in a time-course manner.

☆ *Abbreviations:* BP, blood pressure; LV, left ventricular; EF, ejection fraction; RT, reverse transcription; PCR, polymerase chain reaction; ANP, atrial natriuretic peptide; PAP, pancreatitis-associated protein; DBP, D-binding protein; ET, endothelin; AT, angiotensin.

* Corresponding author. Fax: +81-285-44-7322.
E-mail address: hmano@jichi.ac.jp (H. Mano).

0006-291X/03/$ - see front matter © 2003 Elsevier Inc. All rights reserved.
doi:10.1016/S0006-291X(03)01252-X

To circumvent this hurdle, appropriate model animals would be required, in which hypertension–hypertrophy and heart failure is induced in this order, either naturally or by some treatments. Dahl et al. isolated a mutant strain from Sprague–Dawley rats, which exhibits a genetical hypersensitivity to sodium intake [4]. With a high sodium diet, this "Dahl salt-sensitive" rat developed systemic hypertension and cardiac hypertrophy within a few weeks. Importantly, these changes were followed by the development of congestive heart failure and death in a few months. Therefore, by using the Dahl rats, we could observe how hypertrophy of heart is transformed in vivo into congestive failure.

DNA microarray has revolutionized our way to analyze the gene expression profile. It enables us to monitor the expression level of thousands of genes simultaneously and provides us the "transcriptome" profiles of given cells or tissues [5]. Therefore, DNA microarray would be one of the most suitable approaches to address the gene expression alterations that account for the progression of heart failure. In this paper, we fed Dahl salt-sensitive rats high- or low-sodium diet and compared the transcriptomes of cardiac myocytes at various stages in the affected and control rats. We thereby identified various groups of genes whose expression is dependent on the stage of heart disease.

Materials and methods

Preparation of cardiac myocytes from Dahl salt-sensitive rats. Dahl salt-sensitive rats ($n = 36$) were obtained from Japan SLC (Shizuoka, Japan). They were fed a low-sodium diet (containing 0.3% NaCl) until the age of 6 weeks. Sixteen rats were then switched to a high-sodium diet (containing 8% NaCl), whereas the remaining 20 animals were maintained on the low-sodium diet. Both groups of rats were monitored every week for BP, body weight (BW), thickness of left ventricular (LV) posterobasal free wall, and LV ejection fraction (EF). The latter two were measured by echocardiography (7.5-MHz transducer; Sonos 2000, Hewlett-Packard, Andover, MA) after anesthesia with an intramuscular injection of pentobarbital sodium (15 mg/kg BW). Four rats from each group were killed at ages of 6, 8, 11, 13, and 15 weeks; two of the animals were subjected to pathological examination and the other two were used as a source of LV muscle for DNA microarray analysis.

RNA preparation and DNA microarray analysis. Total RNA was extracted from the LV specimens with the use of RNAzol B (Tel-Test, Friendswood, TX), and a portion (20 μg) was converted to double-stranded cDNA by the SuperScript Choice System (Life Technologies, Gaithersburg, MD) with the T7–dT primer (5′-TCTAGTCGA CGGCCAGTGAATTGTAATACGACTCACTATAGGGCGTTTT TTTTTTTTTTTTTTTT-3′). Biotin-labeled cRNA was prepared from the resulting cDNA with the use of ENZO BioArray RNA labeling kit (ENZO Diagnostics, Farmingdale, NY) and hybridized with the GeneChip Rat U34A array (Affymetrix, Santa Clara, CA) harboring the oligonucleotides corresponding to 8799 genes. Washing of the arrays and detection of the hybridized cRNAs were performed with the GeneChip instrument system according to the manufacturer's protocol.

The fluorescence intensity of each gene was normalized relative to the median fluorescence value for all genes in each chip hybridization. Statistical analysis of the digitized data was performed with GeneSpring 4.0 software (Silicon Genetics, Redwood, CA).

All array data as well as the information for the genes shown in Fig. 3 are available through the web site of *Biochem. Biophys. Res. Commun.*

"Real-time" reverse transcription-polymerase chain reaction (RT-PCR) analysis. Portions of the double-stranded cDNAs were subjected to PCR with SYBR Green PCR Core Reagents (PE Applied Biosystems, Foster City, CA). Incorporation of the SYBR Green dye into the PCR products was monitored in real time with an ABI PRISM 7700 sequence detection system (PE Applied Biosystems), resulting in the calculation of threshold cycle, or C_T value, that defines the PCR cycle number at which an exponential growth of PCR products begins. The C_T values for glyceraldehyde-3-phosphate dehydrogenase (GAPDH) gene and for genes of interest were used to calculate the abundance of the transcripts of these latter genes relative to that of GAPDH mRNA. The oligonucleotide primers for PCR were 5′-ACCACAGTCCAT GCCATCAC-3′ and 5′-TCCACCACCCTGTTGCTGTA-3′ for GAPDH cDNA, 5′-GGTAGGATTGACAGGATTGGAGCC-3′ and 5′-ACATCGATCGTGATAGATGAAGAC-3′ for atrial natriuretic peptide (ANP) cDNA, 5′-TATACCTGGATTGGACTCCATGAC-3′ and 5′-CTTGACAGGATGTGCTTCAGGACA-3′ for pancreatitis-associated protein (PAP) cDNA, 5′-CATCACCATGTGCATCTTC ACGTG-3′ and 5′-AGGAGCCAAACGACATTTATCTGG-3′ for 12-lipoxygenase cDNA, and 5′-GCCTCAGCCAATCATGAAGAAG GC-3′ and 5′-TAGCGTGAAAGCACAGCACGGTAG-3′ for D-binding protein (DBP) cDNA. Amplification of the target products with these primers was verified prior to the real-time PCR analysis.

Results

Development of cardiac hypertrophy and heart failure in Dahl salt-sensitive rats

Dahl salt-sensitive rats were fed either a high- or low-sodium diet and their cardiovascular parameters were monitored. The initial systolic BP at 6 weeks of age was 108.5 ± 11.4 mmHg (mean ± SD, $n = 36$). Animals on the high-sodium diet, however, exhibited a rapid increase in BP to 163.8 ± 9.2 and 227.1 ± 19.6 mmHg after 2 and 4 weeks, respectively, whereas the systolic BP of rats maintained on the low-sodium diet remained within the normal range (121.9 ± 4.3 mmHg after 4 weeks) (Fig. 1A).

In parallel with the progression of systemic hypertension, LV wall thickness also rapidly increased with sodium loading (Fig. 1B). Within 2 weeks of high sodium intake, LV weight per tibial bone length (LVW/TL) changed from 118.12 ± 5.0 to 203.9 ± 9.3 mg/cm, while that of the low-sodium group slowly increased to 142.2 ± 4.9 mg/cm during this time interval.

Although the development of systemic hypertension and cardiac hypertrophy was rapid and almost simultaneous, the pumping function of hearts in the high-sodium group remained normal up to 11 weeks of age (Fig. 1C). Thereafter, however, the LV EF of these animals became rapidly impaired; $85.6 \pm 2.1\%$, $71.1 \pm 3.5\%$, and $61.0 \pm 1.0\%$ at 11, 13, and 15 weeks of age, respectively. In contrast, the EF of rats in the low-sodium group remained at a high level ($87.0 \pm 0.9\%$ at

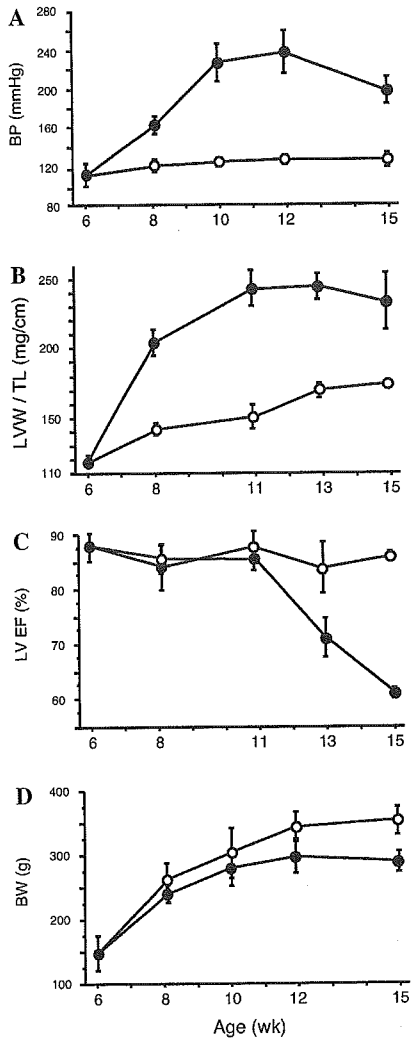

Fig. 1. Disease progression in Dahl salt-sensitive rats. Changes in systolic BP (A), LVW/TL (B), LV EF (C), and BW (D) in Dahl salt-sensitive rats fed a diet containing 8% NaCl (closed circle) or 0.3% NaCl (open circle) from the age of 6 weeks are shown as mean values ± SD ($n = 4$ to 36).

15 weeks of age). The appetite of rats decreased upon the onset of heart failure and the previous steady increase in BW ceased at this stage (Fig. 1D). Most of the animals with the high-sodium intake died between 15 and 18 weeks of age.

It should be noted that pumping failure developed after a certain interval of hypertrophic stage, which resembles well the clinical course in human heart diseases. Patients with a high BP maintain a high LV EF at an early stage of disease; many of them, however, eventually undergo heat failure despite clinical treatment. Therefore, investigation of the transition process from cardiac hypertrophy to heart failure in Dahl salt-sensitive rats may provide us clues to the molecular events essential for the progression to heart failure.

Pathological examination of the Dahl salt-sensitive rats also supported our hypothesis that those with the high-sodium diet well follow the natural course of heart failure in humans. In contrast to the LV myocytes of rats at 6 weeks of age, those from animals subjected to sodium overload for 2 weeks (8 weeks old) exhibited marked hypertrophy (Figs. 2A and B). Furthermore, cross-sections of the sodium-loaded rats at 15 weeks of age clearly demonstrated the feature characteristic to the failed heart in humans; a decrease in the number of viable myocytes, an increase in the amount of fibrotic tissue, and lymphocyte infiltration (Fig. 2C). None of these changes associated with hypertrophy or heart failure were observed in the specimens from the rats with low-sodium intake (data not shown).

Genes induced with the development of hypertension/ hypertrophy

LV tissue samples were prepared from two rats at 6 weeks old (normal stage), and from the ones with the high-sodium diet at 8 weeks old (early hypertension stage), 11 weeks old (late hypertension stage), 13 weeks old (early heart failure stage), and 15 weeks old (late heart failure stage). The samples were also obtained from the age-matched controls with the low-sodium diet and all of them were subjected to DNA microarray analysis. The mean expression level for each gene calculated from the GeneChip data of the two rats was used for statistical analysis.

To visualize the expression levels of the >8000 genes in LV cells at each stage, we here generated a dendrogram, or "gene tree," in which genes of similar expression pattern during the disease progression are placed nearby. The extent of such similarity was measured by the standard correlation with a separation ratio of 0.5 (Fig. 3A). From this tree, it is apparent that the transcriptomes of LV cells from 6-, 8-, and 11-week-old rats fed the low-sodium diet are similar to each other. Statistical "two-way clustering" [6] of the samples also grouped these three samples within the same branch (data not shown). In contrast, observed in this figure were a number of gene clusters that were induced in the rats with sodium overload at 8 weeks or 11 weeks of age.

A total of four genes (seven independent spot-groups on the array) were identified by the extraction of genes whose expression is highly induced in sodium-loaded rats at 8 weeks of age (early hypertrophic stage) compared with that in the age-matched controls (Fig. 3B). It may be notable that these genes can be separated into two sub-groups; one containing only the gene for ANP and the other containing the genes for β-actin, myosin heavy chain polypeptide 7, and aldolase A. While the gene for ANP was induced throughout the entire course, expression of the genes in the latter group decreased lately (at 13 or 15 weeks of age).

We next tried to isolate a group of genes whose expression level in the sodium-loaded rats at 11 weeks of

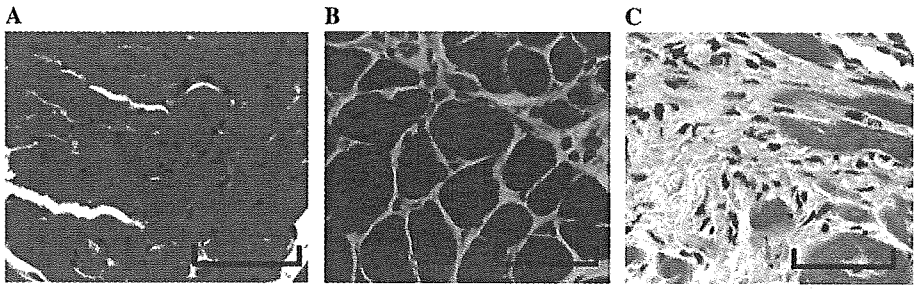

Fig. 2. Pathological examination of LV specimens at normal, hypertrophic, and failing stages of heart disease. Dahl salt-sensitive rats at the normal stage (6 weeks old) (A), hypertrophic stage (8 weeks old) (B), and heart failure stage (15 weeks old) (C) were sacrificed, and the cross-sections of their left ventricles were stained with hematoxylin and eosin. Scale bars, 50 μm.

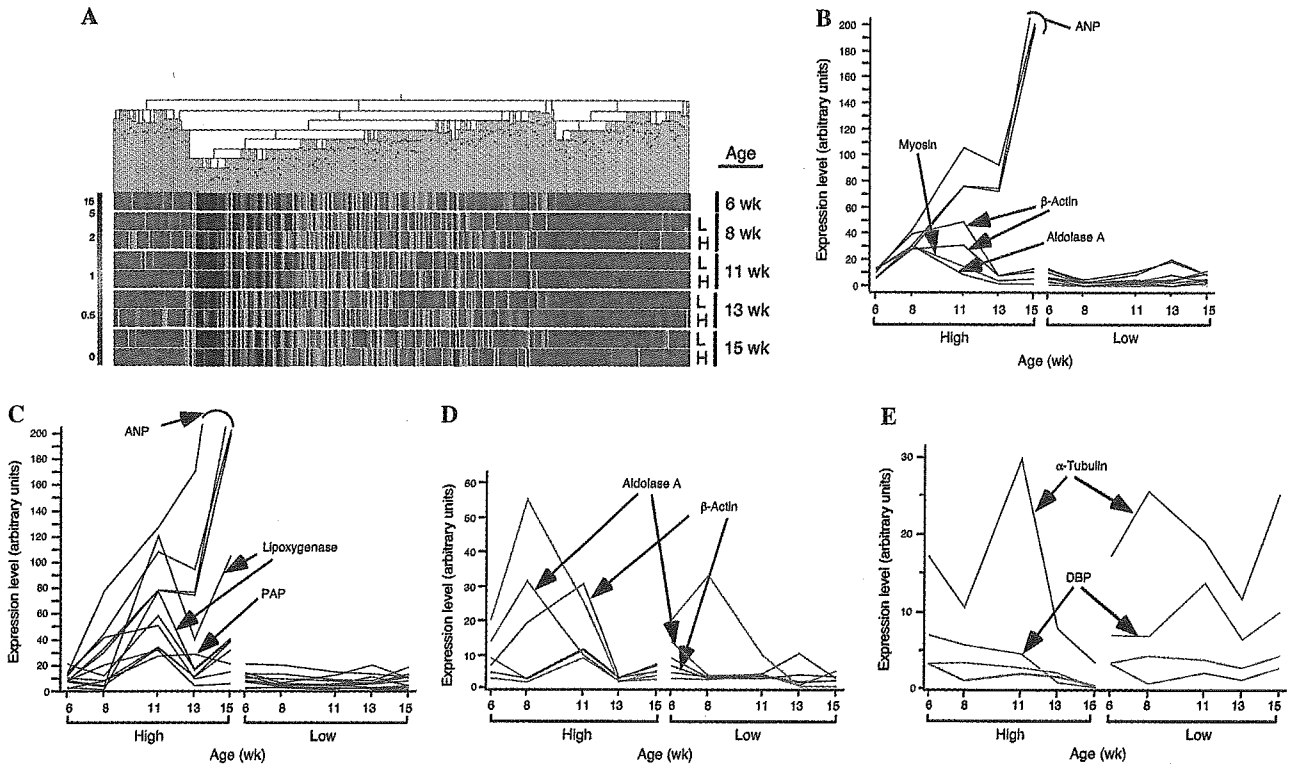

Fig. 3. Identification of genes expressed in a disease stage-specific manner. (A) Expression profiles of >8000 rat genes are shown as a dendrogram in which genes with similar expression pattern across the samples are positioned close to each other. RNA used for the analysis was obtained from rats of the indicated ages that were fed a diet low (L) or high (H) in sodium from 6 weeks of age. The fluorescence intensity of each gene was normalized relative to the mean value for all genes in each hybridization and is shown pseudocolored according to the scale on the left. (B) Expression profiles throughout the observation period for genes whose expression level at 8 weeks of age was markedly increased in rats fed the high-sodium diet (High) compared with that in animals fed the low-sodium diet (Low). Each curve corresponds to a single gene on the GeneChip and is color-coded according to the expression level at 8 weeks of age. Curves corresponding to the genes for ANP, myosin heavy chain polypeptide 7 (Myosin), β-actin, and aldolase A are indicated by arrows. (C) Expression profiles of genes whose expression level at 11 weeks of age was markedly increased in sodium-loaded rats compared with that in control animals. The curves are color-coded according to the expression level at 11 weeks of age. Curves corresponding to the genes for ANP, 12-lipoxygenase, and PAP are indicated. (D) Expression profiles of genes whose expression level increased at the hypertrophic stage (8–11 weeks of age) and decreased thereafter in the rats fed the high-sodium diet. The curves are color-coded according to the expression level at 13 weeks of age. Curves corresponding to the genes for aldolase A and β-actin are indicated. (E) Expression profiles of genes whose expression level decreased with the onset of heart failure in rats fed the high-sodium diet. The curves are color-coded according to the expression level in the sodium-loaded rats at 15 weeks of age. Curves corresponding to the genes for α-tubulin and DBP are indicated. The gene names and accession numbers as well as the expression intensity data for the genes shown in (B)–(E) are available through the web site of Biochem. Biophys. Res. Commun.

age (late hypertrophic stage) was highly induced compared to that in the age-matched controls. Seven genes (12 independent spot-groups on the array) were thus isolated (Fig. 3C). In addition to the four genes extracted above, the newly identified genes included those for PAP and 12-lipoxygenase.

Genes down-regulated along with the reduction in EF

Which genes are activated or down-regulated specifically in the heart failure stage? Our effort to isolate genes whose expression is only induced at this stage has resulted in failure. Therefore, we next focused on genes, expression of which was down-regulated in parallel with the reduction in EF.

For this purpose we attempted to extract genes with two distinct expression patterns. In one group, the genes were silent or expressed at a low level at the normal stage, became activated at the hypertrophic stage, but whose expression subsequently decreased at the heart failure stage. In the next group, the genes were active throughout the normal and hypertrophic stages, but became inactivated at the onset of heart failure (13 weeks of age).

We identified six genes whose expression profiles conformed to the first of these two patterns. The expression of all six genes was thus markedly down-regulated between 11 and 13 weeks of age in rats fed the high-salt diet (Fig. 3D). The expression of, for example, the β-actin gene was elevated throughout the hypertrophic stage (8–11 weeks of age), but became negligible once pumping failure began. The aldolase A gene showed a similar expression profile. Interestingly, neither of them was highly expressed in the rats on the low-sodium diet. Therefore, the expression level of these genes may reflect the contractile ability of LV muscles.

We identified four genes, including those for α-tubulin and DBP, whose expression profiles conformed to the second pattern (Fig. 3E). In contrast to the other two genes in this group, α-tubulin and DBP expressions were active throughout the normal and hypertrophic stages in both sodium-loaded and control rats, but declined only in the sodium-loaded group at the heart failure stage. In other words, the expression level of the two genes changed approximately in a parallel manner to the EF level.

Confirmation of expression level by real-time RT-PCR

We then quantified the mRNA level of the above genes by another method, real-time PCR. The abundance of ANP, 12-lipoxygenase, PAP, and DBP genes was determined relative to that of GAPDH mRNA in the LV specimens obtained from the rats with high- or low-sodium diet. Consistent with the results obtained by microarray analysis, the expression of ANP was kept increased throughout the study only in the sodium-loaded rats (Fig. 4A). Similarly, the real-time PCR confirmed the expression data for the other genes with the GeneChip system. The genes for 12-lipoxygenase (Fig. 4B) and PAP (Fig. 4C) started to increase at 11 weeks of age in the rats with high-sodium diet, but not with the low-sodium one. As shown in Fig. 4D, the expression of DBP was down-regulated along with the progression of heart failure, while it remained at a high

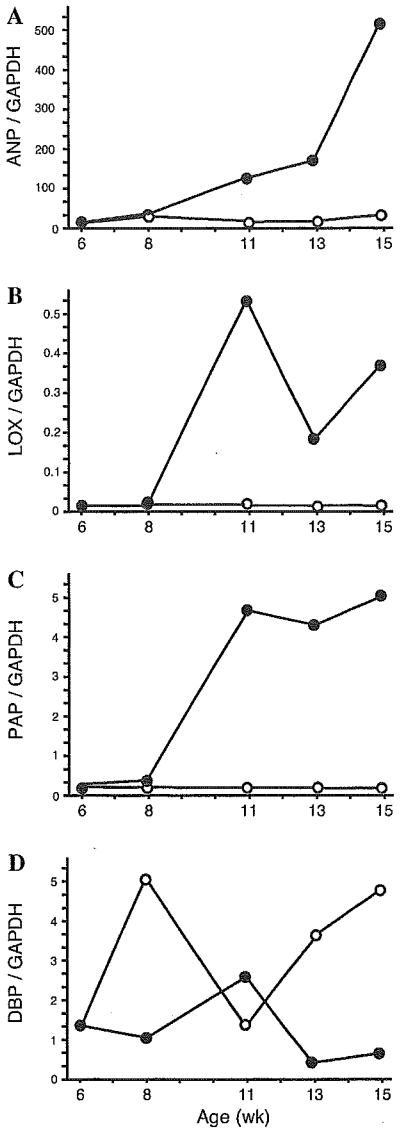

Fig. 4. Quantification of mRNA level by real-time PCR method. The cDNA prepared from LV tissue of Dahl salt-sensitive rats at the indicated ages after being fed a diet containing 8% NaCl (closed circles) or 0.3% NaCl (open circles) was subjected to real-time PCR analysis with primers specific for ANP (A), 12-lipoxygenase (LOX) (B), PAP (C), DBP (D), or GAPDH genes. The ratio of the abundance of the target transcripts to that of GAPDH mRNA was calculated as 2^n, where n is the C_T value for GAPDH cDNA minus the C_T value of the target cDNA.

level during the corresponding period in the rats with low-sodium diet (the reason for the transient decrease in the amount of this mRNA at 11 weeks of age in the control rats is not clear). Thus, overall, the results of the GeneChip analysis correlated well to those obtained by real-time RT-PCR method.

Discussion

In this paper, we have investigated the changes in expression level of a large number of genes in heart

muscles during the disease progression from normal state to cardiac hypertrophy, and subsequently to heart failure in Dahl salt-sensitive rats.

Although the genetic mutation(s) responsible for the salt-sensitivity of these animals remains to be identified, renal cross-transplantation experiment indicated that the primary defect to cause hypertension in the rats should reside within kidney [7]. Actually, feeding the rats a high-sodium diet induces marked changes in kidney morphology, leading to renal dysfunction [8]. Various studies have also implicated the renin–angiotensin (AT) system [9], calcinurin [10,11], endothelin (ET)-system [9,12], and interleukin (IL)-1β [13] in the development of LV hypertrophy and/or heart failure in Dahl salt-sensitive rats.

However, in the present screening, no significant difference was found between the rat LV muscles with the high-sodium and low-sodium intake for the expression levels of AT receptor genes, calcinurin-related genes, ET-related genes, and IL-1β, at least, for the genes included on the GeneChip U34A array (data not shown). Although our data do not exclude the possibility that any of the factors above are involved in the process of hypertrophy or pumping failure, these observations open the possibility of another primary cause which is turned on only in the sodium-overloaded state and evokes the catastrophe of cardiac function.

We could isolate many groups of genes whose expression behavior is highly dependent on the amount of sodium in the diet. For instance, expression of the ANP gene differed most markedly between the sodium-loaded and control rats; its expression was kept increased to the final stage in the rats fed the high-sodium diet, but remained negligible in the rats on the low-sodium one (Figs. 3B and C). ANP is a vasodilator released from atrium in response to pressure overload, but was also shown to be expressed in ventricle [14]. The pronounced increase in ANP gene expression observed in the present study may therefore result from the systemic hypertension and congestive heart failure that developed in sodium-loaded rats.

The increase in β-actin and myosin heavy chain gene expression observed during the development of hypertrophy likely reflects the associated increase in cardiac muscle mass and contractile ability. Consistent with this notion, the expression of both of these genes subsequently decreased with the progression to heart failure (Fig. 3B). It would also be possible that the increase of aldolase A gene is considered in the same context. Aldolase A is a ubiquitous protein and functions in the glycolysis process. Therefore, induction of aldolase A may reflect the elevated catabolic activity in the hypertrophic muscles. Diminution of its expression in the failure stage is compatible with this hypothesis.

The 12-lipoxygenase protein catalyzes the transfer of oxygen to the C-12 position of arachidonic acid. Although its in vivo function is not clear yet, it is of interest that the products of this enzyme may have a growth promoting activity [15,16]. The gene expression of 12-lipoxygenase is, at least partially, under the control of angiotensin II stimulation, and the metabolite of this enzyme can induce hypertrophy of vascular smooth muscle cells. Furthermore, Gabel et al. [17] indicated the cardioprotective effect of 12-lipoxygenase. Thus, overexpression of this gene only in the sodium-loaded rats may contribute to the development of hypertrophy, and the transient inactivation of the gene at the age of 13 weeks (Figs. 3C and 4B) may be related to the transition to the heart failure state.

PAP, also known as HIP [18], is known to be released from pancreas upon pancreatitis [19] and is related to C-type lectins. Based on its structural motifs, PAP is supposed to be involved in the cell-to-cell contact or cell migration, while its specific role in vivo is totally unknown. Functional role of sustained expression of PAP only in the rats with the high-sodium diet also remains to be elucidated.

From this study, the gene of potential interest may be that for DBP which belongs to the basic region-leucine zipper (bZIP) family of transcriptional factors [20]. Close relatives to DBP include thyrotroph embryonic factor (TEF) [21], hepatic leukemia factor (HLF) [22], and NFIL3/E4BP4 [23]. These proteins are likely to play a pivotal role in the determination of cell fate for apoptosis [24], and, thus, it was an interesting finding that DBP was constantly expressed at a high level in the rats with the low-sodium diet, but that the expression of DBP became down-regulated along with the progression of heart failure only in the sodium-loaded rats. It would be an intriguing question whether DBP functions for cardioprotective effect.

In conclusion, our study has provided new insight into the molecular mechanisms of cardiac hypertrophy and heart failure. Additional screening to identify genes whose expression is altered specifically at the heart failure stage should further increase our understanding of this condition.

Acknowledgments

We are grateful to T. Kanbe for her excellent technical assistance. This work was supported in part by a Grant-in-Aid for Scientific Research on Priority Areas (C) "Medical Genome Science" from the Ministry of Education, Science, Sports and Culture of Japan.

References

[1] M.A. James, A.M. Saadeh, J.V. Jones, Wall stress and hypertension, J. Cardiovasc. Risk 7 (2000) 187–190.

[2] E. Braunwald, Shattuck lecture–cardiovascular medicine at the turn of the millennium: triumphs, concerns, and opportunities, New. Engl. J. Med. 337 (1997) 1360–1369.
[3] J. Scheuer, Catecholamines in cardiac hypertrophy, Am. J. Cardiol. 83 (1999) 70H–74H.
[4] J.P. Rapp, S.M. Wang, H. Dene, A genetic polymorphism in the renin gene of Dahl rats cosegregates with blood pressure, Science 243 (1989) 542–544.
[5] D.J. Duggan, M. Bittner, Y. Chen, P. Meltzer, J.M. Trent, Expression profiling using cDNA microarrays, Nat. Genet. 21 (1999) 10–14.
[6] U. Alon, N. Barkai, D.A. Notterman, K. Gish, S. Ybarra, D. Mack, A.J. Levine, Broad patterns of gene expression revealed by clustering analysis of tumor and normal colon tissues probed by oligonucleotide arrays, Proc. Natl. Acad. Sci. USA 96 (1999) 6745–6750.
[7] L.K. Dahl, M. Heine, Primary role of renal homografts in setting chronic blood pressure levels in rats, Circ. Res. 36 (1975) 692–696.
[8] R.B. Sterzel, F.C. Luft, Y. Gao, J. Schnermann, J.P. Briggs, D. Ganten, R. Waldherr, E. Schnabel, W. Kriz, Renal disease and the development of hypertension in salt-sensitive Dahl rats, Kidney Int. 33 (1988) 1119–1129.
[9] K. Yamamoto, T. Masuyama, Y. Sakata, T. Mano, N. Nishikawa, H. Kondo, N. Akehi, T. Kuzuya, T. Miwa, M. Hori, Roles of renin–angiotensin and endothelin systems in development of diastolic heart failure in hypertensive hearts, Cardiovasc. Res. 47 (2000) 274–283.
[10] W. Hayashida, Y. Kihara, A. Yasaka, S. Sasayama, Cardiac calcineurin during transition from hypertrophy to heart failure in rats, Biochem. Biophys. Res. Commun. 273 (2000) 347–351.
[11] Y. Sakata, T. Masuyama, K. Yamamoto, N. Nishikawa, H. Yamamoto, H. Kondo, K. Ono, K. Otsu, T. Kuzuya, T. Miwa, H. Takeda, E. Miyamoto, M. Hori, Calcineurin inhibitor attenuates left ventricular hypertrophy, leading to prevention of heart failure in hypertensive rats, Circulation 102 (2000) 2269–2275.
[12] Y. Iwanaga, Y. Kihara, K. Hasegawa, K. Inagaki, T. Yoneda, S. Kaburagi, M. Araki, S. Sasayama, Cardiac endothelin-1 plays a critical role in the functional deterioration of left ventricles during the transition from compensatory hypertrophy to congestive heart failure in salt-sensitive hypertensive rats, Circulation 98 (1998) 2065–2073.
[13] T. Shioi, A. Matsumori, Y. Kihara, M. Inoko, K. Ono, Y. Iwanaga, T. Yamada, A. Iwasaki, K. Matsushima, S. Sasayama, Increased expression of interleukin-1 beta and monocyte chemotactic and activating factor/monocyte chemoattractant protein-1 in the hypertrophied and failing heart with pressure overload, Circ. Res. 81 (1997) 664–671.
[14] A. Rosenzweig, C.E. Seidman, Atrial natriuretic factor and related peptide hormones, Annu. Rev. Biochem. 60 (1991) 229–255.
[15] R. Natarajan, N. Gonzales, L. Lanting, J. Nadler, Role of the lipoxygenase pathway in angiotensin II-induced vascular smooth muscle cell hypertrophy, Hypertension 23 (1994) 1142–1147.
[16] J.L. Gu, H. Pei, L. Thomas, J.L. Nadler, J.J. Rossi, L. Lanting, R. Natarajan, Ribozyme-mediated inhibition of rat leukocyte-type 12-lipoxygenase prevents intimal hyperplasia in balloon-injured rat carotid arteries, Circulation 103 (2001) 1446–1452.
[17] S.A. Gabel, R.E. London, C.D. Funk, C. Steenbergen, E. Murphy, Leukocyte-type 12-lipoxygenase-deficient mice show impaired ischemic preconditioning-induced cardioprotection, Am. J. Physiol. Heart Circ. Physiol. 280 (2001) 1963–1969.
[18] C. Lasserre, L. Christa, M.T. Simon, P. Vernier, C. Brechot, A novel gene (HIP) activated in human primary liver cancer, Cancer Res. 52 (1992) 5089–5095.
[19] V. Keim, J.L. Iovanna, B. Orelle, J.M. Verdier, M. Busing, U. Hopt, J.C. Dagorn, A novel exocrine protein associated with pancreas transplantation in humans, Gastroenterology 103 (1992) 248–254.
[20] C.R. Mueller, P. Maire, U. Schibler, DBP, a liver-enriched transcriptional activator, is expressed late in ontogeny and its tissue specificity is determined posttranscriptionally, Cell 61 (1990) 279–291.
[21] D.W. Drolet, K.M. Scully, D.M. Simmons, M. Wegner, K.T. Chu, L.W. Swanson, M.G. Rosenfeld, TEF, a transcription factor expressed specifically in the anterior pituitary during embryogenesis, defines a new class of leucine zipper proteins, Genes Dev. 5 (1991) 1739–1753.
[22] T. Inaba, W.M. Roberts, L.H. Shapiro, K.W. Jolly, S.C. Raimondi, S.D. Smith, A.T. Look, Fusion of the leucine zipper gene HLF to the E2A gene in human acute B- lineage leukemia, Science 257 (1992) 531–534.
[23] I.G. Cowell, A. Skinner, H.C. Hurst, Transcriptional repression by a novel member of the bZIP family of transcription factors, Mol. Cell. Biol. 12 (1992) 3070–3077.
[24] S. Ikushima, T. Inukai, T. Inaba, S.D. Nimer, J.L. Cleveland, A.T. Look, Pivotal role for the NFIL3/E4BP4 transcription factor in interleukin 3- mediated survival of pro-B lymphocytes, Proc. Natl. Acad. Sci. USA 94 (1997) 2609–2614.

Oncogene (2003) 22, 5720–5728

www.nature.com/onc

Proteomic analysis of hematopoietic stem cell-like fractions in leukemic disorders

Jun Ota[1,9], Yoshihiro Yamashita[1,9], Katsuya Okawa[1], Hiroyuki Kisanuki[1], Shin-ichiro Fujiwara[1,3], Madoka Ishikawa[1], Young Lim Choi[1], Shuichi Ueno[1,4], Ruri Ohki[1,4], Koji Koinuma[1,5], Tomoaki Wada[1,6], Duane Compton[7], Toshihiko Kadoya[8] and Hiroyuki Mano*[,1]

[1]*Division of Functional Genomics, Jichi Medical School, 3311-1 Yakushiji, Kawachi-gun, Tochigi 329-0498, Japan;* [2]*Pharmaceutical Research Laboratories, Pharmaceutical Division, Kirin Brewery Co. Ltd, Takasaki, Gunma 370-1925, Japan;* [3]*Division of Hematology, Jichi Medical School, Kawachi-gun, Tochigi 329-0498, Japan;* [4]*Division of Cardiology, Jichi Medical School, Kawachi-gun, Tochigi 329-0498, Japan;* [5]*Department of Surgery, Jichi Medical School, Kawachi-gun, Tochigi 329-0498, Japan;* [6]*Department of Gynecology, Jichi Medical School, Kawachi-gun, Tochigi 329-0498, Japan;* [7]*Department of Biochemistry, Dartmouth Medical School, Hanover, NH 03755-3844, USA;* [8]*R&D Center, Product Department, Pharmaceutical Division, Kirin Brewery Co. Ltd, Maebashi, Gunma 371-0853, Japan*

DNA microarray analysis has been applied to identify molecular markers of human hematological malignancies. However, the relatively low correlation between the abundance of a given mRNA and that of the encoded protein makes it important to characterize the protein profile directly, or 'proteome,' of malignant cells in addition to the 'transcriptome.' To identify proteins specifically expressed in leukemias, here we isolated AC133$^+$ hematopoietic stem cell-like fractions from the bone marrow of 13 individuals with various leukemic disorders, and compared their protein profiles by two-dimensional electrophoresis. A total of 11 differentially expressed protein spots corresponding to 10 independent proteins were detected, and peptide fingerprinting combined with mass spectrometry of these proteins revealed them to include NuMA (nuclear protein that associates with the mitotic apparatus), heat shock proteins, and redox regulators. The abundance of NuMA in the leukemic blasts was significantly related to the presence of complex karyotype anomalies. Conditional expression of NuMA in a mouse myeloid cell line resulted in the induction of aneuploidy, cell cycle arrest in G_2–M phases, and apoptosis. These results demonstrate the potential of proteome analysis with background-matched cell fractions obtained from fresh clinical specimens to provide insight into the mechanism of human leukemogenesis.
Oncogene (2003) **22,** 5720–5728. doi:10.1038/sj.onc.1206855

Keywords: acute myeloid leukemia; proteome; AC133; NuMA

*Correspondence: H Mano; E-mail: hmano@jichi.ac.jp
[9]These two authors contributed equally to this work
Received 7 February 2003; revised 23 May 2003; accepted 9 June 2003

Introduction

Annotation of the draft sequence of the human genome has opened up the possibility of applying novel genomic approaches to the characterization of molecular pathogenesis of human disorders (The genome international sequencing consortium, 2001; Venter *et al.*, 2001). Among genomic screening methods, DNA microarray analysis has to date provided the greatest insight into leukemogenesis. This technology readily allows measurement of the expression levels of thousands of genes simultaneously (Duggan *et al.*, 1999). Expression profiling with microarrays has thus made it possible, for example, to distinguish acute myeloid leukemia (AML) from acute lymphoid leukemia (ALL) (Golub *et al.*, 1999), to define novel subgroups of leukemias and lymphomas (Alizadeh *et al.*, 2000; Armstrong *et al.*, 2002), and to identify candidate genes for leukemogenesis (Ohmine *et al.*, 2001; Makishima *et al.*, 2002).

An important concern in the assay of fresh specimens by microarray analysis, however, is that apparent changes in gene expression detected at different stages of carcinogenesis may actually reflect changes in cell composition rather than changes in gene expression *per se*. For example, whereas immature (leukemic) blasts constitute $\geqslant$20% of bone marrow (BM) mononuclear cells (MNCs) in individuals with leukemia, BM MNCs of normal individuals contain only a few percent immature blasts. A simple comparison by microarray analysis between normal and leukemic BM cells would, therefore, likely reveal changes in gene expression only attributable to the expansion of immature blasts in the latter. Indeed, we observed that one of the genes whose expression appeared highly specific for leukemic BM cells, compared with normal BM cells, was that for CD34, simply reflecting the expansion of CD34$^+$ leukemic blasts in the leukemic BM specimen (Miyazato *et al.*, 2001).

To eliminate such population-shift effects, we have purified and stored AC133$^+$ hematopoietic stem cell (HSC)-like fractions from the BM of patients with a wide range of leukemic disorders and deposited them in our 'Blast Bank.' The suitability of such purified fractions for microarray analysis was confirmed by the observation that the CD34 gene was expressed at similar levels in AC133$^+$ cells obtained from normal individuals and in those isolated from leukemic patients (Miyazato *et al.*, 2001). Microarray analysis of Blast Bank samples has also resulted in the identification of new molecular markers for myelodysplastic syndrome (MDS) (Miyazato *et al.*, 2001) and for chronic myeloid leukemia (CML) (Ohmine *et al.*, 2001).

Despite its potential for identifying genes important in leukemogenesis, microarray analysis is not able to provide direct information on the abundance or post-translational modification of proteins. The transcriptional activity on a given gene is thus not always a major determinant of the expression level of the encoded protein. After exclusion of several of the most abundant proteins, a large-scale study (Gygi *et al.*, 1999) of yeast cells determined the correlation coefficient between the amount of an mRNA and the abundance of the corresponding protein to be only $\sim$0.4. Furthermore, only four out of 28 proteins identified in a mouse cell line showed relative levels similar to those of the corresponding mRNAs (Lian *et al.*, 2001). A thorough characterization of leukemogenesis thus requires direct determination of the accompanying changes not only in the amounts of cellular mRNAs but also in protein abundance.

In addition to discrepancies between the amounts of mRNA and protein derived from a given gene, the activities of many proteins are influenced by post-translational modifications such as phosphorylation, cleavage, glycosylation, and redox regulation. Such concerns have highlighted the importance of proteomic approaches that are able to assess changes in the abundance and post-translational modification of proteins on a large scale. One of the main current strategies in proteomics is the combination of two-dimensional gel electrophoresis (2DE) and mass spectrometry (MS). Whereas 2DE allows the screening of hundreds to thousands of proteins for changes in molecular size, isoelectric point (pI), or phosphorylation, MS then allows the identification of protein spots of interest.

However, as in the case of DNA microarray analysis, the population-shift effect is also an important consideration in proteomics. Differentiation of cells is thus accompanied by changes in the expression of a substantial number of proteins (Lian *et al.*, 2001). A proteome comparison between two specimens with different cell compositions would therefore yield pseudopositive data that reflect only the population-shift effect. A proteomic approach to the characterization of leukemogenesis would thus ideally require the purification of background-matched cell populations from fresh specimens of leukemic patients.

We have now prepared protein extracts from the purified AC133$^+$ leukemic blasts of 13 individuals with acute leukemia or related disorders. Screening of these protein samples with 2DE and MS resulted in the identification of 10 proteins that were expressed differentially among the patients.

Results

2DE of Blast Bank samples

Our goal was to identify proteins whose abundance, relative molecular mass, or pI differs markedly among HSC-like fractions isolated from individuals with leukemia. Preliminary studies with cell lines revealed that at least 1×10^6 MNCs were required to yield $\geqslant$100 spots reproducibly on 2DE gels. Given that the AC133$^+$ HSC-like fraction usually constitutes a small proportion of leukemic blasts, it was not always possible to obtain such a large number of AC133$^+$ cells from fresh patient specimens. Indeed, our Blast Bank contained only 13 AC133$^+$ fractions that comprised $\geqslant 2 \times 10^6$ cells. The clinical characteristics of the corresponding patients (five with *de novo* AML, four with MDS-associated AML, three with myeloproliferative disorders (MPDs) in blast crisis (BC), and one with ALL) are summarized in Table 1. All these patients died within 12 months of diagnosis.

Our preliminary studies also revealed that abundant proteins sometimes masked neighboring minor protein spots on the 2DE gels. To minimize such effects, we therefore first fractionated the cell samples into different subcellular components, including nuclear, mitochondrial, microsomal, and cytosolic fractions (Watarai *et al.*, 2000). Each subcellular fraction was then independently compared by 2DE among the 13 patients. The cytosolic fractions consistently yielded $\geqslant$100 spots per gel and were analysed further in the present study. The comparisons of the other subcellular fractions will be described separately.

Identification of differentially expressed proteins

A representative image of a silver-stained gel, for which Melanie III software detected >200 independent spots, is shown in Figure 1a. Comparison of these spots among the gel images for the 13 patients revealed a total of 11 spots that showed a significant difference in abundance (as judged by the criteria described in Materials and methods). Peptide fingerprinting by matrix-assisted laser desorption-ionization time-of-flight (MALDI-TOF) MS of these 11 spots resulted in the identification of the corresponding 10 proteins (Table 2). They include nuclear protein that associates with the mitotic apparatus (NuMA), heat shock 70-kDa protein 5 (HSPA5), heat shock 70-kDa protein 8 (HSPA8), adenosine deaminase (ADA), aldolase A (ALDOA), triose phosphate isomerase 1 (TPI1), glutathione S-transferase pi (GST-pi), superoxide dismutase 2 (SOD2), peptidyl-prolyl isomerase A (PPIA), and heat shock 70-kDa protein 9B (HSPA9B). Two independent spots with different molecular mass and pI values were revealed to

Table 1 Clinical characteristics of the patients subjected to proteome analysis

Patient ID	*Age (years)*	*Sex*	*Disease and subtype*	*Treatment outcome*	*Abnormal chromosomes (⩾3)*
AML #1	65	M	AML, M0	Failure	−
AML #2	71	M	AML, M0	Failure	+
AML #3	65	F	AML, M1	CR	−
AML #4	31	F	AML, M4	Failure	−
AML #5	83	F	AML, M5a	Failure	−
MDS #1	69	M	MDS-associated AML, M2	Failure	−
MDS #2	67	F	MDS-associated AML, M2	Failure	+
MDS #3	68	F	MDS-associated AML, M4	Failure	−
MDS #4	53	M	MDS-associated AML, M2	Failure	+
MPD #1	60	M	MPD, BC	Failure	+
MPD #2	68	F	PV, BC	Failure	+
MPD #3	33	M	CML, BC	Failure	−
ALL #1	23	F	ALL, L1	Failure	−

FAB subtypes for the patients are indicated. Abbreviations: M, male; F, female; CR, complete remission; PV, polycythemia vera

be derived from the same gene product, HSPA8 (Figure 1a).

We then examined whether clinical parameters of the patients were related to the intensity of any of the 11 protein spots. The expression level of NuMA was significantly related to whether the number of abnormal chromosomes was $\geqslant 3$ or <3 ($P=0.017$; Student's *t*-test). The images of the NuMA spots for all 13 patients are shown in Figure 1b. NuMA is a nuclear protein that accumulates in the pericentrosomal region of the mitotic spindle and plays an important role in the assembly of mitotic asters (Compton and Cleveland, 1993; Gaglio *et al.*, 1997; Du *et al.*, 2001).

Since we could obtain only several thousands of $AC133^+$ cells from the BM aspirates of healthy volunteers, it was impossible to assess the protein level of $p240^{NuMA}$ directly in the $AC133^+$ fractions of normal individuals. Instead, here we have quantified the abundance of *NuMA* mRNA by the 'real-time' reverse transcription–polymerase chain reaction (RT–PCR) method. The abundance of *NuMA* mRNA relative to that of glyceraldehyde-3-phosphate dehydrogenase (GAPDH) mRNA was examined among the $AC133^+$ HSC-like fractions obtained from a healthy volunteer and those with CML in chronic phase (CP), in addition to the specimens subjected to 2DE (Figure 1c). Although the mRNA level of *NuMA* did not precisely correlate with the corresponding protein level, there was a tendency that its mRNA was abundant in the samples with a high expression of NuMA protein (shown in gray columns).

The proportion of malignant blasts is below 5% in BM MNCs of patients with CML in CP, and, therefore, such BM aspirates could yield only $1\times10^3\sim1\times10^4$ of $AC133^+$ cells, which were not enough for the protein analysis. However, since these patients had only one chromosomal anomaly, t(9;22), they were chosen to be included in this RT–PCR analysis. The expression level of the *NuMA* gene was negligibly low in the HSC-like fractions of a normal individual and most patients with CML in CP, which indirectly supports the low expression of NuMA protein in these specimens.

Aneuploidy associated with NuMA expression

The role of NuMA in mitosis suggested that aberrant induction of NuMA expression in leukemic blasts might contribute to the chromosomal instability apparent in such cells. To examine directly the effects of NuMA overexpression, we transfected mouse myeloid 32D cells (Greenberger *et al.*, 1983) with a vector that confers Zn^{2+}-dependent expression of human NuMA. Cell clones transfected with this vector (32D-NuMA#1 to 32D-NuMA#7) or the corresponding empty vector (32D-MT#1 to 32D-MT#4) were selected by culture in the presence of G418, after which 0.1 mM Zn^{2+} was added to the culture medium. Immunoblot analysis with antibodies to NuMA revealed marked expression of $p240^{NuMA}$ in the 32D-NuMA clones, but not in the 32D-MT clones (Figure 2a). The electrophoretic mobility of NuMA expressed in the 32D-NuMA clones was identical to that of $p240^{NuMA}$ detected in human kidney 293 cells transiently transfected with the pMT-NuMA vector.

The Zn^{2+} dependence of NuMA expression in each 32D-NuMA clone was verified by incubating cells in the absence or presence of $ZnSO_4$. Immunoblot analysis revealed a marked dependence of NuMA expression on the presence of Zn^{2+} for all 32D-NuMA clones (Figure 2b; data not shown). The amount of NuMA in 32D-NuMA#1 cells, for example, incubated overnight in the absence or presence of Zn^{2+} was 12.8 and 59.8 times, respectively, that of endogenous $p240^{NuMA}$ in 32D-MT cells.

Examination of the morphology of 32D transfectants revealed that the induction of NuMA expression in some cells resulted in a marked increase in cell size and in the formation of multiple nuclei (Figure 3a); effects suggestive of the development of aneuploidy. Flow cytometric analysis of DNA content revealed that incubation of 32D-NuMA transfectants with Zn^{2+} for 2 days led to mitotic block (a decrease in the proportion of cells in S phase of the cell cycle, and an increase in the proportion of those in G_2–M); such an effect was not observed in 32D-MT cells (Table 3). Furthermore, induction of NuMA expression in transfected cells was

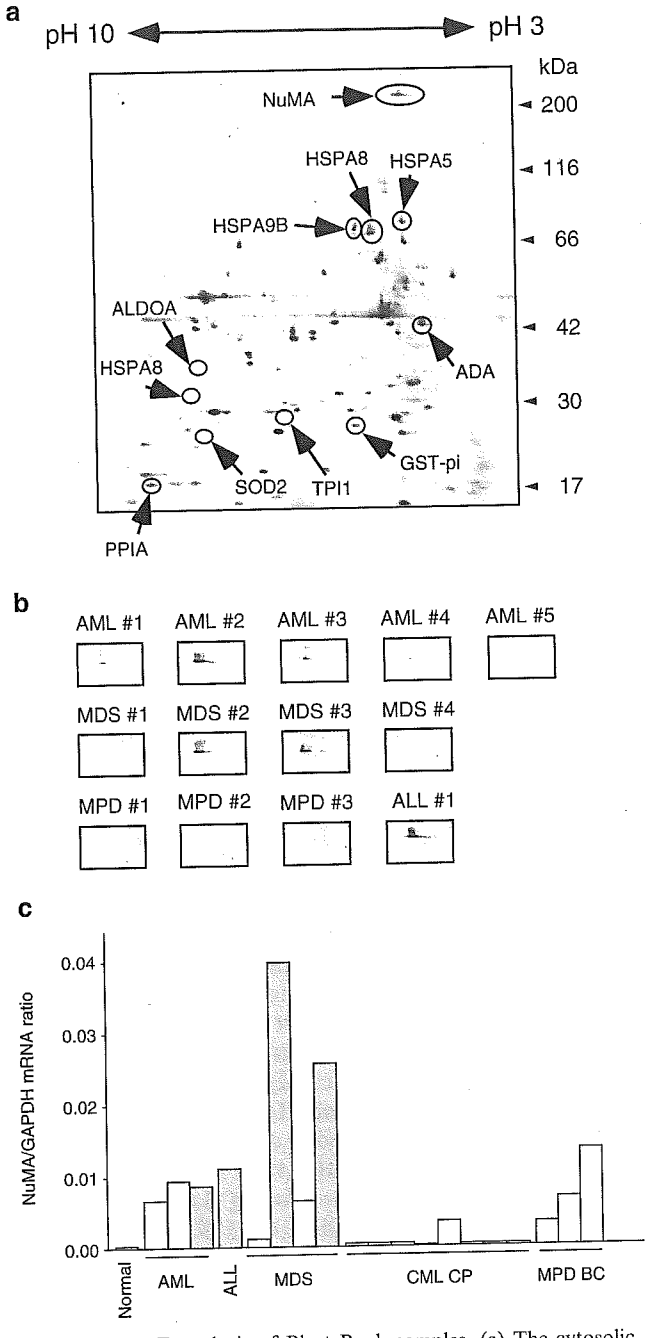

Figure 1 2DE analysis of Blast Bank samples. (**a**) The cytosolic fraction (~10 μg of protein) isolated from AC133$^+$ leukemic blasts was subjected to 2DE on a 7.5–15% gradient gel. The scanned image of the silver-stained gel was then used to detect and compare protein spots. The positions and identities of proteins expressed differentially among leukemic patients are indicated by arrows, and the positions of molecular mass standards (in kilodaltons) are shown on the right. (**b**) Images of the NuMA spots for all 13 patients analysed. (**c**) Complementary DNAs were prepared from the AC133$^+$ blasts of a healthy volunteer (normal) and those with AML, ALL, MDS-associated leukemia (MDS), CML in CP, and MPD in BC, and were subjected to real-time RT–PCR analysis with primers specific for the *NuMA* or *GAPDH* gene. The ratio of the abundance of *NuMA* mRNA to that of *GAPDH* mRNA was calculated as 2^n, where n is the C_T value for *GAPDH* cDNA minus the C_T value for *NuMA* cDNA. The expression levels of *NuMA* mRNA for the patients with abundant expression of NuMA proteins (more than 3.0 U in Table 2) are shown as gray columns

associated with an increase in the proportion of cells with an abnormal (4(n)) DNA content (Table 4). These data thus suggested that overexpression of NuMA perturbs cell cycle progression by inhibiting mitosis and thereby results in the development of aneuploidy.

We also noticed that induction of p240^{NuMA} expression was accompanied by the appearance of cells with apoptotic features (Figure 3a) as well as by marked decreases in both the rate of cell growth (Figure 3b) and cell viability (data not shown). The increase in the prevalence of apoptosis in NuMA-overexpressing cells was confirmed by the detection of an increased extent of internucleosomal DNA fragmentation by agarose gel electrophoresis of genomic DNA (Figure 3c).

In our 2DE analysis, NuMA was identified within the cytoplasmic fractions, while the protein was originally reported to be accumulated in the nucleus. To determine its subcellular localization, p240^{NuMA} fused with enhanced green fluorescent protein (EGFP) (NuMA-EGFP) was expressed in human kidney 293 cells. As shown in Figure 3d, EGFP was expressed diffusely within cells. With regard to NuMA-EGFP, it was localized in the nucleus (but not in the nucleolus) in the majority of transfected cells (NuMA-EGFP#1). There was, however, a fraction of cells that had NuMA exclusively within their cytoplasm (NuMA-EGFP#2–3). Therefore, NuMA can be localized within the cytoplasm in living cells. Since such cells with cytoplasmic NuMA had a round shape, they may be at specific stages of the cell cycle. It would be an intriguing issue to address whether subcellular localization of p240^{NuMA} is regulated in a cell cycle-dependent manner.

Discussion

We have compared the protein profiles of HSC-like fractions derived from individuals with various leukemia-related disorders. Given that the proteome is strongly influenced by cell differentiation (Lian *et al.*, 2002), a simple comparison of BM MNCs from different patients is likely to result in the identification of proteins whose apparent change in expression actually reflects a difference in the cellular composition of the specimens. To prevent such a complication, we isolated highly immature BM cells on the basis of their surface expression of AC133. Comparison of such background-matched fractions should eliminate pseudopositive data that might result from different proportions of leukemic blasts in BM or from differences in cell lineage to which the leukemic blasts are committed (Miyazato *et al.*, 2001).

We identified 10 proteins that were expressed differentially among the leukemic blasts from the 13 patients examined. Three of these proteins (HSPA5, HSPA8 and HSPA9B) belong to the heat shock protein family of 70 kDa (HSP70), and two of them (GST-pi and SOD2) function in redox regulation. HSPA5 (also known as glucose-regulated protein 78 (GRP78) or immunoglobulin heavy chain-binding protein (BiP)), HSPA8 (heat

Table 2 Quantitation of the abundance of proteins expressed differentially among the patients

Protein	*Accession number*	*Patient ID*												
		AML #1	*AML #2*	*AML #3*	*AML #4*	*AML #5*	*MDS #1*	*MDS #2*	*MDS #3*	*MDS #4*	*MPD #1*	*MPD #2*	*MPD #3*	*ALL #1*
NuMA	XP_006005	1.339	8.135	1.350	0.324	0.700	0.492	10.771	4.772	0.460	0.780	0.139	0.177	7.100
HSPA5	P11021	0.378	0.347	0.801	0.391	0.579	0.374	0.424	0.063	0.100	0.396	0.827	0.582	0.478
HSPA8 (p71)	P11142	1.440	0.569	2.554	1.442	0.328	1.107	0.677	0.236	0.180	0.673	0.324	0.793	1.150
ADA	P00813	0.113	0.900	1.859	0.530	0.500	1.007	1.104	1.618	1.178	2.750	1.688	0.236	0.766
ALDOA	P04075	0.264	1.336	0.119	0.164	0.843	0.324	0.970	1.723	0.436	0.144	0.280	0.218	0.630
HSPA8 (p34)	P11142	0.150	0.786	0.081	0.158	0.435	0.490	0.108	0.582	0.000	0.306	0.553	0.071	0.191
TPI1	P00938	0.743	2.061	0.727	0.262	1.254	2.162	0.464	2.990	0.157	0.602	0.439	0.605	0.903
GST-pi	P09211	0.785	0.737	1.312	0.841	2.107	0.685	0.302	1.241	0.290	0.660	1.276	1.077	0.868
SOD2	P04179	0.083	0.283	0.065	0.562	0.290	0.325	0.096	0.341	0.000	0.336	0.143	0.594	0.255
PPIA	P05092	1.473	1.630	0.924	0.147	1.534	2.008	0.905	0.733	1.722	2.006	0.175	0.884	0.567
HSPA9B	P38646	0.253	0.206	0.779	1.688	0.215	0.550	0.231	0.148	0.325	0.445	0.446	0.317	0.175

Normalized spot intensity (arbitrary units) as well as accession numbers for the Entrez protein database (http://www.ncbi.nlm.nih.gov/entrez/) are shown for the differentially expressed proteins

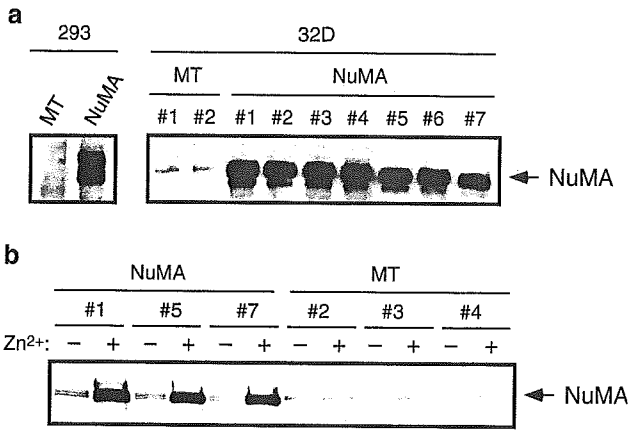

Figure 2 Conditional expression of NuMA in 32D cells. (**a**) Stable transfectants of 32D cells were isolated for pMT-CB6 (MT) or pMT-NuMA (NuMA) vectors. Total cell lysates (10 μg of protein per lane) prepared from cells incubated overnight in the presence of 0.1 mM $ZnSO_4$ were subjected to immunoblot analysis with antibodies to NuMA. Total cell lysates prepared from human kidney 293 cells transiently transfected with pMT-CB6 or pMT-NuMA were similarly analysed. The position of $p240^{NuMA}$ is indicated on the right. (**b**) The transfected 32D clones were cultured overnight with (+) or without (−) $ZnSO_4$ and then analysed for the induction of NuMA expression as in (**a**)

shock cognate protein 70 (HSC70), HSP73, or lipopolysaccharide-associated protein 1 (LAP1)), and HSPA9 (HSP75, mortalin, or GRP75) all function as molecular chaperones. Their expression is induced by a variety of cellular stressors and they are thought to facilitate protein folding and oligomerization. In addition, however, whereas forced expression of one of the two isoforms of HSPA9, HSPA9A (MOT1), induces cell senescence (Kaul *et al.*, 1995), that of HSPA9B (MOT2), which differs from HSPA9A by only two amino acids, promotes cell cycle progression and malignant transformation (Kaul *et al.*, 1998). Although it is not known how MOT proteins induce malignant transformation, the stress-induced tyrosine phosphorylation of these proteins suggests that they function downstream of protein tyrosine kinases. Many molecular chaperones have also been shown to possess antiapoptotic activity (Jaattela, 1999). An increased expression of HSP70 family proteins in leukemic blasts might thus be directly linked to leukemogenesis or to the development of resistance to chemotherapeutic drugs.

The redox state of cells reflects a precise balance between the production of reactive oxygen species and the activity of reducing agents, the latter of which include thiol-based buffers and SOD (Davis *et al.*, 2001). GST functions in cellular detoxification by catalysing the conjugation of reduced glutathione (GSH) to target molecules. In addition, GST-pi has been linked to chemoresistance to doxorubicin (Volm *et al.*, 1992) and to cisplatin (Okuyama *et al.*, 1994), and GST isoforms have been shown to be directly regulated by c-Jun NH_2-terminal kinase (JNK), also known as stress-activated protein kinase (SAPK) (Adler *et al.*, 1999). SOD2, also known as manganese-dependent SOD (MnSOD), is a mitochondrial enzyme that catalyses dismutation of the superoxide anion into O_2 and H_2O_2. Overexpression of this enzyme has been detected in cancer cells (Pang *et al.*, 1997) as well as in neurons of individuals with autosomal recessive parkinsonism (Matsumine *et al.*, 1997; Shimoda-Matsubayashi *et al.*, 1997). It remains to be determined whether an increased expression of GST-pi or SOD2 contributes to leukemogenesis.

NuMA was one of the most abundant soluble proteins in the leukemic blasts from some of the patients analysed in the present study. Given that NuMA is essential for the formation of the mitotic spindle, our observation that the abundance of this protein in leukemic blasts was related to the number of chromosomal abnormalities suggested that aberrant NuMA activity might result in a failure of cells to complete mitosis and lead to the development of chromosomal instability. We indeed demonstrated such effects of NuMA by inducing its expression in mouse 32D cells. However, the forced expression of NuMA also resulted in G_2–M arrest and apoptosis. The mere overexpression of NuMA does not therefore appear to be sufficient for malignant transformation to leukemic cells. Other genetic events that promote cell cycle progression or

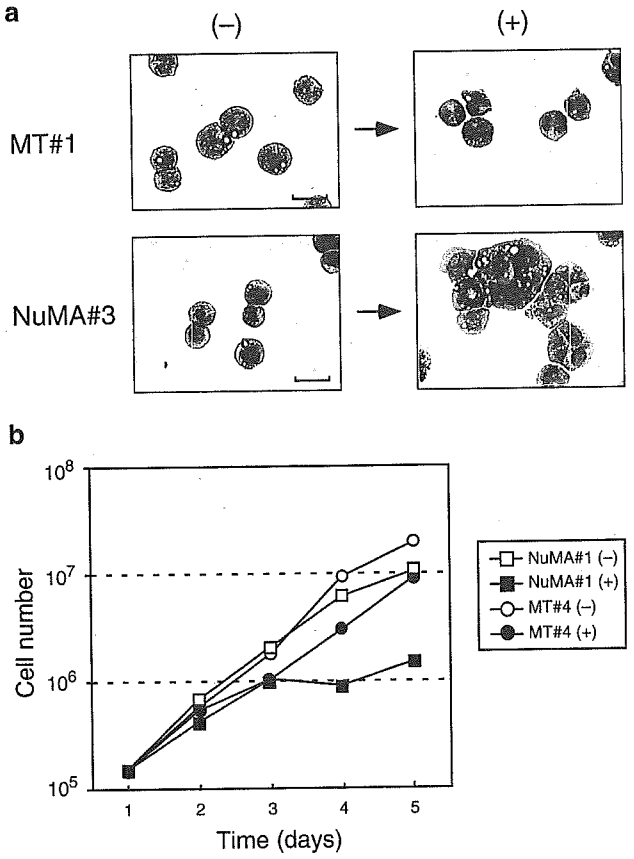

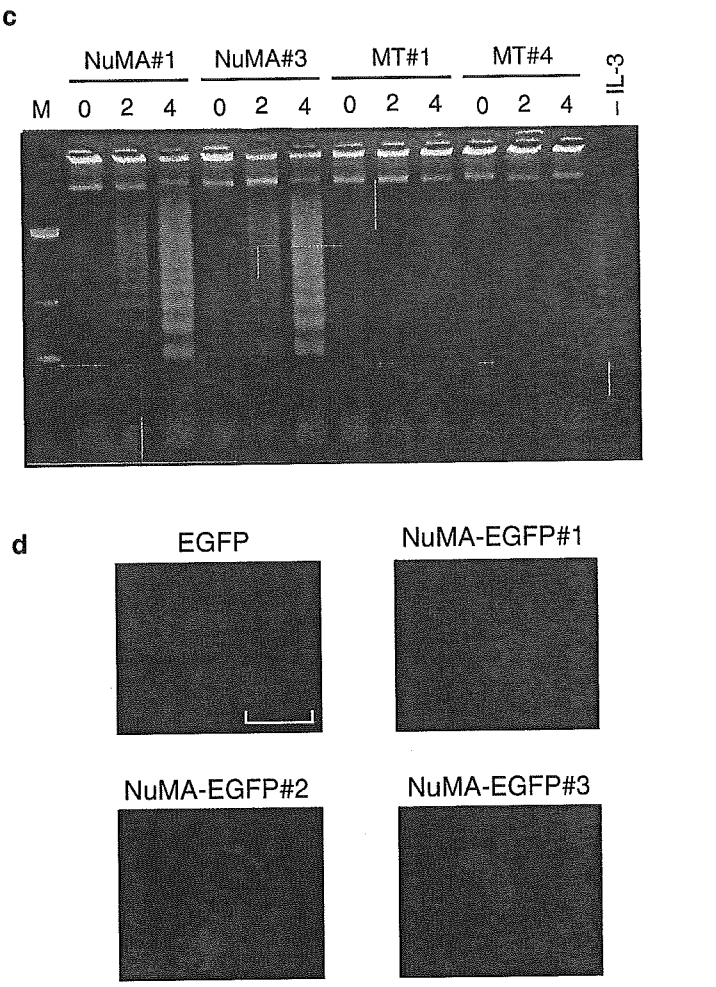

Figure 3 Induction of aneuploidy and apoptosis by expression of $p240^{NuMA}$. (**a**) Mouse 32D cell clones transfected with pMT-CB6 (MT#1) or pMT-NuMA (NuMA#3) were cultured for 4 days in RPMI 1640 medium supplemented with 10% FBS and IL-3 (25 U/ml) either in the absence (–) or presence (+) of 0.1 mM $ZnSO_4$. The cells were then stained with Wright–Giemsa solution and examined by light microscopy. Scale bar; 30 μm. (**b**) Mouse 32D cell clones transfected with pMT-CB6 (MT#4) or pMT-NuMA (NuMA#1) were cultured as in (**a**) in the absence (–) or presence (+) of $ZnSO_4$, and total cell number was determined at the indicated times. (**c**) Mouse 32D cell clones transfected with pMT-CB6 (MT#1 and #4) or pMT-NuMA (NuMA#1 and #3) were cultured as in (**a**) in the presence of IL-3 and $ZnSO_4$ for 0, 2, or 4 days, as indicated. Genomic DNA was then isolated, subjected to agarose gel electrophoresis through a 2% gel, and stained with ethidium bromide. Genomic DNA was also examined for 32D cells in which apoptosis was induced by an overnight deprivation of IL-3 (rightmost lane). Lane M, DNA size markers (50-bp ladder, Invitrogen). (**d**) Human kidney 293 cells transfected with pEGFP (EGFP) or pEGFP/NuMA (NuMA-EGFP#1–3) were subjected to the analysis with a fluorescent microscope. Scale bar; 20 μm

protect cells from apoptosis are likely also required to overcome the proapoptotic activity of NuMA. Chromosomal instability associated with NuMA expression may increase the chance of such genetic events, the occurrence of which may be reflected in changes in the proteome detected in our study.

Current proteomics techniques are limited in their sensitivity for protein detection. In our study, no single 2DE image yielded >300 independent protein spots, which is far fewer than the total number of human proteins predicted from sequencing of the human genome (30 000–40 000 proteins without taking into account the products of alternative RNA splicing). Further improvements in proteomics tools and their application to the direct comparison of protein profiles among background-matched cell fractions prepared from fresh specimens should provide an insight into the intracellular events that underlie malignant transformation in human leukemias.

Figure 3 Continued

Table 3 Cell cycle analysis of NuMA-expressing cells

		Cells (%)		
Clone	*Time with Zn^{2+} (days)*	*G_1*	*S*	*G_2–M*
MT#1	0	29.5	63.1	7.4
	2	27.5	60.5	12.0
NuMA#1	0	31.2	61.1	7.7
	2	33.1	28.9	38.1
NuMA#3	0	30.6	61.0	7.8
	2	31.9	35.2	32.9

Mouse 32D cells transfected with pMT-NuMA (NuMA#1 and #3) or pMT-CB6 (MT#1) were incubated with 0.1 mM $ZnSO_4$ for the indicated times, after which the percentage of cells in G_1, S, or G_2–M phase of the cell cycle was determined by flow cytometry

Table 4 Effect of NuMA induction on the proportion of cells with aneuploidy

Clone	*Time with Zn^{2+} (days)*	*4(n) fraction (%)*
MT#1	0	1.98
	2	1.96
	4	1.35
MT#4	0	1.86
	2	1.11
	4	1.63
NuMA#1	0	1.47
	2	4.87
	4	3.97
NuMA#3	0	1.65
	2	5.59
	4	4.51

Mouse 32D cells transfected with pMT-NuMA (NuMA#1 and #3) or pMT-CB6 (MT#1 and #4) were incubated for the indicated times with 0.1 mM $ZnSO_4$, after which the percentage of cells with an increased DNA contents (4(*n*)) was determined flow cytometry

Materials and methods

Cell culture

Mouse myeloid 32D cells were cultured in RPMI 1640 medium (Invitrogen, Carlsbad, CA, USA) supplemented with 10% fetal bovine serum (FBS) and mouse interleukin-3 (IL-3; 25 U/ml; Invitrogen). Cells transfected with pMT-CB6-based vectors were subjected to selection with the same medium containing G418 (1 mg/ml; Invitrogen). Human kidney 293 cells (American Type Culture Collection) were cultured in DMEM/F12 medium (Invitrogen) supplemented with 10% FBS and 1 mM L-glutamine.

Isolation of Blast Bank samples

With written informed consent, BM MNCs had been isolated by Ficoll-Hypaque density gradient centrifugation from the individuals with various hematopoietic disorders. $AC133^+$ cells were purified from such MNCs and stored in our Blast Bank with the use of an immunoaffinity chromatography for AC133 as described previously (Miyazato *et al.*, 2001). Briefly, MNCs were labeled with magnetic bead-conjugated antibody toward AC133 (AC133 MicroBeads; Miltenyi Biotec, Auburn, CA, USA) in phosphate-buffered saline supplemented with 3% FBS and 2 mM EDTA. The cells were then loaded onto miniMACS magnetic cell separation columns (Miltenyi Biotec), and $AC133^+$ cells were purified according to the manufacturer's instruction. To examine the enrichment of $AC133^+$ cells, portions of the MNC and $AC133^+$ cell preparations were stained with Wright-Giemsa solution or analysed with a FACScan flow cytometer (Becton Dickinson, Mountain View, CA, USA) for the expression of CD34, CD38, and AC133. At the end of March 2003, Blast Bank contained 411 independent $AC133^+$ fractions, including 141, 95, and 60 specimens derived from individuals with de novo AML, MDS, or CML, respectively.

2DE of subcellular fractions

A total of 13 $AC133^+$ cell preparations (2×10^6–1×10^7 cells) were subjected to subcellular fractionation by sequential centrifugation as described previously (Watarai *et al.*, 2000). In brief, cells were suspended in 300 μl of a solution containing 20 mM HEPES-NaOH (pH 7.4) and 0.25 M sucrose, and homogenized by 30 strokes in a Dounce homogenizer. The resulting homogenate was centrifuged at 1000 *g* for 10 min, the resulting pellet was saved as the nuclear fraction, and the resulting supernatant was further centrifuged at 10 000 *g* for 10 min. The pellet from this second centrifugation was saved as the mitochondrial fraction, and the supernatant was centrifuged at 100 000 *g* for 60 min to yield the microsomal fraction (pellet) and cytosolic fraction (supernatant). All subcellular fractions were independently subjected to isoelectric focusing on IPG DryStrips (pH 3–10 NL; Amersham Biosciences, Uppsala, Sweden) with a Multiphor II electrophoresis system (Amersham Biosciences). The separated proteins were then subjected to SDS–PAGE through 7.5–15% gradient gels (Bio-Craft, Tokyo, Japan) and visualized by silver staining (Shevchenko *et al.*, 1996).

Protein identification

Stained gels were scanned with an LAS1000 image analyser (Fujifilm, Tokyo, Japan) to generate a digitized image file. Protein spots in the image were detected with the use of Melanie III software (GeneBio, Geneva, Switzerland) with manual adjustment, and were quantified by the same software. The intensity of each spot on a gel was normalized on the basis of the total signal intensity for that gel. The total number of spots detected in one gel image was 168 ± 59 (mean $\pm$ s.d.). A protein spot was classified as differentially expressed if (1) the intensity of the spot was $\geqslant 0.5$ arbitrary units in at least one of the 13 image files and (2) the spot intensity ratio was $\geqslant 5$ for comparison between any pair of gel images. The 11 spots that fulfilled these criteria were excised from the gels and subjected to protease digestion and peptide fingerprinting by MALDI-TOF MS (Voyager ET STR; Applied Biosystems, Foster City, CA, USA). The determined molecular masses of peptides were compared with an in-house nonredundant protein database maintained by Kirin Brewery Co. Ltd.

Quantitative real-time RT–PCR analysis

Total RNA was extracted from the purified $AC133^+$ cells with the use of RNAzol B (Tel-Test, Inc., Friendswood, TX, USA), and a portion of the RNA was converted to double-stranded cDNA by the SuperScript Choice System (Life Technologies, Gaithersburg, MD, USA). The cDNAs were then subjected to PCR with a QuantiTect SYBR Green PCR Kit (Qiagen, Valencia, CA, USA). The amplification protocol comprised incubations at 94°C for 15 s, 60°C for 30 s (54°C in the case of *NuMA* cDNA), and 72°C for 60 s. Incorporation of the SYBR Green dye into PCR products was monitored in real time with an ABI PRISM 7700 sequence detection system (PE Applied Biosystems, Foster City, CA, USA), thereby allowing determination of the threshold cycle (C_T) at which exponential amplification of PCR products begins. The C_T values for cDNAs corresponding to *GAPDH* and *NuMA* genes were used to calculate the abundance of *NuMA* mRNA relative to that of *GAPDH* mRNA. The oligonucleotide primers for PCR were 5′-GTCAGTGGTGGACCTGACCT-3′ and 5′-TGAGCTT-GACAAAGTGGTCG-3′ for *GAPDH* cDNA, and 5′-AAAA-TAGCCTCATCAGCAGCTTGG-3′ and 5′-CCAGCTTCT-GGCTCTTCTCTGACT-3′ for *NuMA* cDNA.

Conditional expression of NuMA in 32D cells

The full-length cDNA for human NuMA was inserted into the pMT-CB6 vector (kindly provided by T Inaba, Hiroshima University, Hiroshima, Japan), which allows Zn^{2+}-dependent expression of exogenous genes in eucaryotic cells. The resulting pMT-NuMA vector or the empty vector was then introduced into 32D cells by electroporation as described previously